Entomological Lidar

Target Characterization and Field Applications

Jansson, Samuel

2020

Document Version:
Publisher's PDF, also known as Version of record

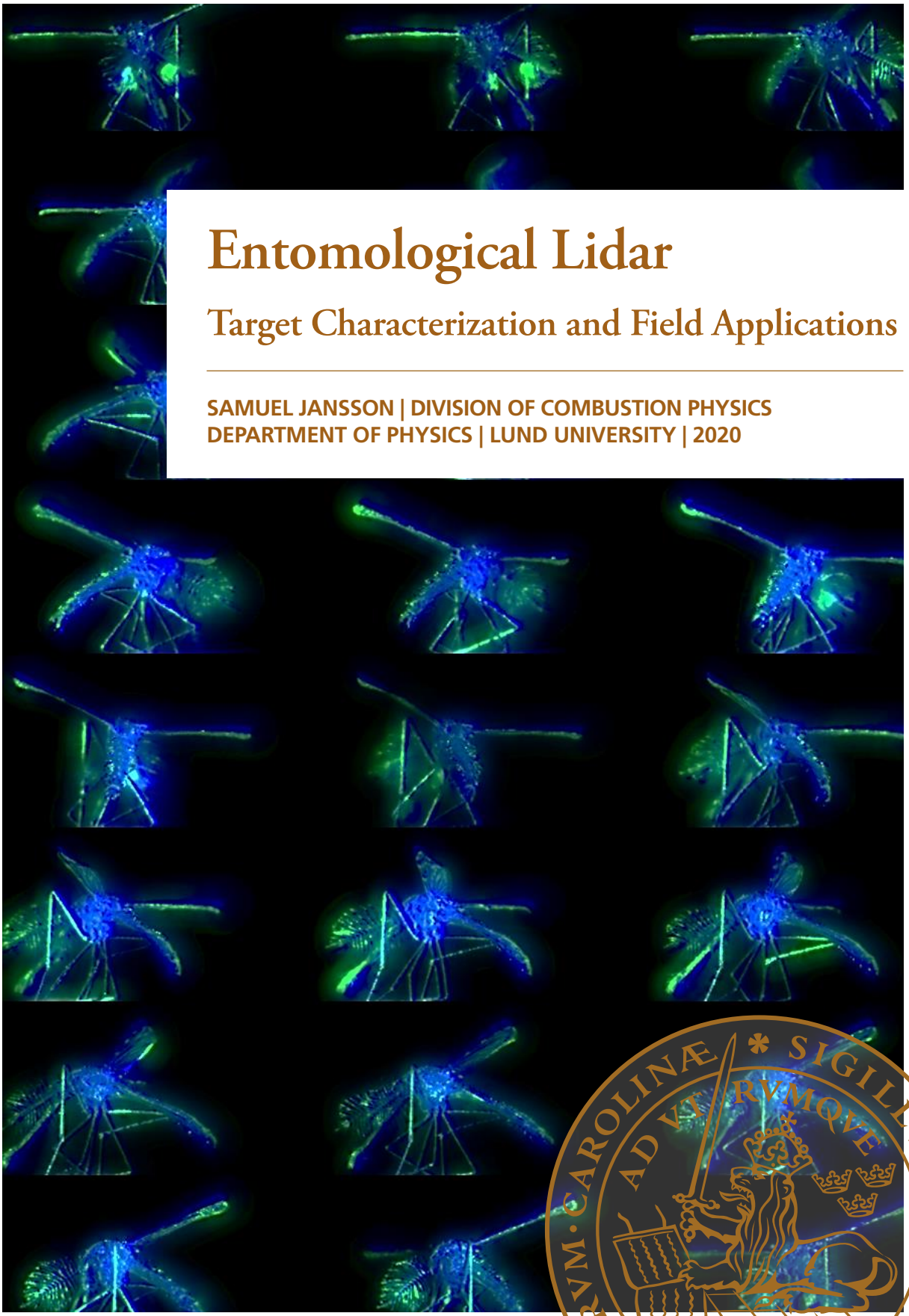

Entomological Lidar

Target Characterization and Field Applications

SAMUEL JANSSON | DIVISION OF COMBUSTION PHYSICS
DEPARTMENT OF PHYSICS | LUND UNIVERSITY | 2020

Entomological Lidar

Target Characterization and Field Applications

Samuel Jansson

LUND
UNIVERSITY

DOCTORAL DISSERTATION

by due permission of the Faculty of Engineering, Lund University, Sweden.
To be defended at Rydbergsalen, Fysicum, Professorsgatan 1.
February 14th at 09:15.

Faculty opponent
Prof. Benjamin P. Thomas, Department of Physics, New Jersey Institute of Technology, Newark, New Jersey, USA

Organization LUND UNIVERSITY Division of Combustion Physics, Department of Physics P.O Box 118, SE-211 00 Lund, Sweden	**Document name** Doctoral Dissertation
	Date of issue: 2020-01-21
	CODEN: LUTFD2/TFCP-217-SE
Author: Samuel Jansson	Sponsoring organization

Title: Entomological Lidar – Target Characterization and Field Applications

Abstract

This thesis treats entomological lidar from various angles: laboratory reference work on insects of interest, methodological development of lidar- and data processing methods, as well as field implementations of lidar techniques for entomological research. Insects are crucial components of ecosystems and are currently in a global decline. In this thesis, insects are mainly studied in their roles as disease vectors and food sources for vertebrates. However, several other feasible application avenues of entomological lidar exist and are touched upon briefly. Entomological lidar is an optical remote sensing technique in which the light scattered by insects is recorded by a sensor and the distance to each insect is derived. In classical lidar, ranging is achieved through time-of-flight detection. In this thesis the Scheimpflug- and passive lidar methods have been used, in which ranging is achieved through triangulation and geometrical optics.

In the laboratory reference work, the light-scattering properties of insects were investigated. Considerable effort has been put into the study of *ex-vivo* and *in-vivo* malaria mosquitoes in search of optical properties that may enable remote species classification. These species otherwise require capture and microscope analysis by an expert to distinguish. Dragonflies have the narrowest spectral bands so far observed in nature. In this PhD work, their scattering properties were investigated and give hints regarding possible uses of these narrow bands.

Methodological development has been pursued for improvement and optimization of instrumentation through simulation and laboratory reference measurements. Hyperspectral images of insects were used to motivate laser wavelength selection based on signal strength, information yield and laser availability. Raytracing was used to devise a passive lidar scheme and to optimise the geometry of Scheimpflug lidars. Data processing techniques for robust and accurate calibration of sizes, wing-beat frequencies with associated modulation spectra, flight headings and dispersal of insects in lidar data were developed.

Entomological lidar techniques were applied in a number of field settings around the world. In Sweden, insect swarms at the nacelle of a wind farm were observed post sunset in weather conditions associated with high bat mortality through collision with wind farms. In China, increased insect activity was observed at the onset of heavy rain. The main crepuscular activity peak of insects was observed in the short time window with decreased predation pressure around sunset, when neither birds nor bats were active. In Africa, an extra activity peak was observed at noon among mosquitoes and other crepuscular insects during a solar eclipse. Male mosquito mating swarms were observed with consistent timing and location each day, and a highly directional dispersal of mosquitoes into a village was observed every evening.

In this thesis work, peak numbers of more than a thousand insects per minute have been observed, resolved temporally and spatially at μs and cm scales, respectively, which is inconceivable with conventional entomological methods. Laboratory reference work and methodological development allow the quantification and classification of insect signals *in-situ*. Thereby, questions of significant ecological importance could be answered.

Key words: Lidar, remote sensing, laser radar, Scheimpflug lidar, entomological lidar

Classification system and/or index terms (if any)

Supplementary bibliographical information	Language: English
ISSN and key title: 1102-8718	ISBN (print): 978-91-7895-418-6 ISBN (pdf): 978-91-7895-419-3
Recipient's notes	**Number of pages:** 297 / Price
	Security classification

Entomological Lidar

Target Characterization and Field Applications

Samuel Jansson

LUND
UNIVERSITY

Front cover photos by Samuel Jansson

Back cover photos by Samuel Jansson, Mikkel Brydegaard and Jens Rydell

Department of Physics
Faculty of Engineering
Lund University

Lund Reports on Combustion Physics, LRCP-221
ISBN 978-91-7895-418-6 (print)
ISBN 978-91-7895-419-3 (pdf)

ISSN 1102-8718
ISRN LUTFD2/TFCP-221-SE

Printed by Tryckeriet i E-huset, Lund 2020

“Science – Is it cool, or is it whack?”

This question was first posed by the great philosopher Ali G.
Despite years of dedicated pursuit, the answer still eludes me.

Table of Contents

List of publications

I. **First Polarimetric Investigation of Malaria Mosquitoes as Lidar Targets**
S. Jansson, P. Atkinson, R. Ignell and M. Brydegaard
IEEE Journal of Selected Topics in Quantum Electronics **25**, 1-8 (2019).

II. **Multiband modulation spectroscopy for determination of sex and species of mosquitoes in flight**
A. Gebru, **S. Jansson**, R. Ignell, C. Kirkeby, J. Prangsma and M.Brydegaard
Journal of Biophotonics **11**, e201800014 (2018).

III. **Correlation of mosquito wing-beat harmonics to aid in species classification and flight heading assessment**
S. Jansson, A. Gebru, R. Ignell, J. Abbott and M. Brydegaard
Proceedings of SPIE **11075**, 110750Q (2019).

IV. **Can the narrow red bands of dragonflies be used to perceive wing interference patterns?**
M. Brydegaard, **S. Jansson**, M. Schulz and A. Runemark
Ecology and Evolution **8**, 5369-5384 (2018).

V. **Passive kHz lidar for the quantification of insect activity and dispersal**
S. Jansson and M. Brydegaard
Animal Biotelemetry **6**, 6 (2018).

VI. **The Scheimpflug lidar method**
M. Brydegaard, E. Malmqvist, **S. Jansson**, J. Larsson, S. Török and G. Zhao
Proceedings of SPIE **10406**, 104060I (2017).

VII. **Advances in entomological laser radar**
M. Brydegaard and **S. Jansson**
The Journal of Engineering **2019**, 7542-7545 (2019).

VIII. **Effective Parameterization of Laser Radar Observations of Atmospheric Fauna**
E. Malmqvist, **S. Jansson**, S. Török and M. Brydegaard
IEEE Journal of Selected Topics in Quantum Electronics **22**, 1-8 (2016).

IX. **Insect abundance over Chinese rice fields in relation to environmental parameters, studied with a polarization-sensitive CW near-IR lidar system**
S. Zhu, E. Malmqvist, W. Li, **S. Jansson**, Y. Li, Z. Duan, K. Svanberg, H. Feng, Z. Song, G. Zhao, M. Brydegaard and S. Svanberg
Applied Physics B **123**, 211 (2017).

X. **Risky bat bait – Insect swarm dynamics at a wind turbine observed with Scheimpflug lidar**
S. Jansson, E. Malmqvist, M. Brydegaard, S. Åkesson and J. Rydell
In review

XI. **The bat-bird-bug battle: daily flight activity of insects and their predators over a rice field revealed by high-resolution Scheimpflug Lidar**
E. Malmqvist, **S. Jansson**, S. Zhu, W. Li, K. Svanberg, S. Svanberg, J. Rydell, Z. Song, J. Bood, M. Brydegaard and S. Åkesson
Royal Society Open Science **5**, 172303 (2018).

XII. **Lidar reveals Activity Anomaly of Malaria Vectors during Pan-African Eclipse**
M. Brydegaard, **S. Jansson**, E. Malmqvist, Y. Mlacha, A. Gebru, F. Okumu, G. Killeen and Carsten Kirkeby
In review

XIII. **Real-time dispersal of malaria vectors in rural Africa monitored with lidar**
S. Jansson, E. Malmqvist, Y. Mlacha, R. Ignell, F. Okumu, G. Killeen, C. Kirkeby and M. Brydegaard
Submitted

Related work

XIV. **Exploitation of Multi-Band Lidar for the Classification of Free-Flying Migratory Birds: a Pilot Study over Athens, Greece**
S. Jansson, A. Papayannis, S. Åkesson, G. Tsaknakis and M. Brydegaard
EPJ Web of Conferences **119**, 27002 (2016).

XV. **Exploitation of an atmospheric lidar network node in single-shot mode for the classification of aerofauna**
S. Jansson, M. Brydegaard, A. Papayannis, G. Tsaknakis and S. Åkesson
Journal of Applied Remote Sensing **11**, 1-14 (2017).

XVI. **Short-wave infrared atmospheric Scheimpflug lidar**
A. Gebru, **S. Jansson**, R. Ignell, C. Kirkeby and M. Brydegaard
EPJ Web of Conferences **176**, 01012 (2018).

XVII. **Multispectral polarimetric modulation spectroscopy for species and sex determination of Malaria disease vectors**
M. Brydegaard, J. Larsson, S. Török, E. Malmqvist, G. Zhao, **S. Jansson**, M. Andersson, S. Svanberg, S. Åkesson, F. Laurell and J. Bood
Proceedings of Conference on Lasers and Electro-Optics (CLEO) (2017).

XVIII. **Insect remote sensing using a polarization sensitive cw lidar system in Chinese rice fields**
S. Zhu, E. Malmqvist, Y. Li, **S. Jansson**, W. Li, Z. Duan, W. Fu, K. Svanberg, J. Bood, H. Feng, S. Åkesson, Z. Song, B. Zhang, G. Zhao, D. Li, M. Brydegaard and S. Svanberg
EPJ Web of Conferences **176**, 07001 (2018).

XIX. **Applications of lidar remote sensing of insects in agricultural entomology on the Chinese scene**
Z. Song, B. Zhang, H. Feng, S. Zhu, L. Hu, M. Brydegaard, Y. Li, **S. Jansson**, E. Malmqvist, K. Svanberg, G. Zhao, J. Bood, S. Svanberg and D. Li
Journal of Applied Entomology **2019**, 1-9 (2019).

XX. **Entomological Scheimpflug lidar for estimating unique insect classes *in situ* – field test from Ivory Coast**
B. Kouakou, **S. Jansson**, M. Brydegaard and J. Zoueu
Submitted

XXI. **Passive remote sensing studies of a phantom insect**
M. Sougoti, **S. Jansson**, S. Kam and M. Brydegaard
In preparation

Patent applications

P1. **An optical remote sensing system for detection of aerial and aquatic fauna**
S. Jansson and M. Brydegaard
International: WO2018078166A1, Application Filing (2018).
Europe: EP3532865A1, Pending (2019).
United States: US20190302265A1, Pending (2019).
China: CN110036310A, Search and Examination (2019).

Populärvetenskaplig sammanfattning

Sin ringa storlek till trots har insekter enorm inverkan på vårt samhälle och våra liv. Bin, som är centrala för att vårt jordbruk ska fungera, har minskat drastiskt i antal de senaste åren. En utbredd bidöd skulle i bästa fall tvinga oss lägga om vår kosthållning markant, och i värsta fall leda till svält. Utöver detta skulle växter som är beroende av bin för sin fortplantning och djur som äter bin löpa stor risk att dö ut. Skadedjur har stor ekonomisk inverkan på jord- och skogsbruk. En stor del av skörden förloras varje år, och majoriteten av alla träd som dör gör det på grund av skadedjur. Insekter sprider även en mängd sjukdomar, i vissa fall med dödligt utfall. Myggan är det mest mordiska djuret på vår planet, och ligger bakom uppemot en miljon dödsfall per år. Fattiga barn på landsbygden i Afrika är den mest utsatta gruppen. Konventionella metoder för att studera insekter inbegriper i många fall att de fångas in med hjälp av olika typer av fällor. Sådana metoder kan ge väldigt bra information om de infångade insekterna, men är arbetskrävande och fångar ett relativt lågt antal insekter. De kan även ge snedvridna resultat på grund av så kallad bias, vilket innebär att den erhållna informationen är inte nödvändigtvis representativ för de insekter som ej fångats in, eller för populationen som helhet. Utöver detta kan metoderna inte mäta exempelvis flygaktivitet, flygriktning och spridning av insekter.

Optiska metoder har under flera decennier tillämpats inom medicin, i fältet biofotonik. Molekyler i biologisk vävnad, såsom melanin och vatten, har olika optiska egenskaper, vilka i stor utsträckning är kända. Optisk fjärranalys är, liksom biofotonik, ett väl etablerat forskningsområde inom vilket gaser och partiklar i atmosfären studeras med hjälp av laserljus. I detta avhandlingsarbete kombineras biofotonik och optisk fjärranalys, och teori och metoder från båda fälten används för att studera insekter på avstånd.

Aktiva metoder (med laserljus) och passiva metoder (med solljus) har utvecklats för att detektera insekter i realtid på flera hundra meters avstånd. För varje observerad insekt beräknas storheter som vingslagsfrekvens med modulationsspektrum, storlek, flyghastighet och flygriktning. Dessa parametrar har sedan använts för att klassificera insekter. När två laserstrålar med olika våglängd används kan vatten- och melaninhalten i en insekt beräknas, och när två laserstrålar med olika polarisation används kan mikrostrukturer undersökas. Utöver dessa fältmetoder har ett flertal laboratoriesystem konstruerats för att undersöka specifika arters optiska egenskaper under kontrollerade former. Dessa

referensmätningar kan sedan användas för att identifiera de undersökta arterna i fält, så att deras beteende kan studeras. Jämfört med konventionella metoder kan långt fler insekter observeras, mätt i tusental per minut. Utöver detta har de utvecklade metoderna avsevärt högre rums- och tidsupplösning, och möjliggör studier av insekters aktivitet och rörelsemönster på helt ny detaljnivå.

Inom ramen för min forskarutbildning har jag använt dessa metoder för att studera insekter i olika sammanhang. Jag har studerat ett flertal insekter i laboratorium, både för att förstå deras optiska egenskaper från ett fysikaliskt perspektiv och för att ta fram referensinformation till fältstudier. Jag har utvecklat mätmetoder och signalbehandlingsmetoder för att klassificera och kartlägga insekter i det fria. Jag har studerat insekter som föda till större djur, såsom fåglar och fladdermöss, för att förstå dynamiken och interaktionen som ligger bakom deras beteende. Slutligen har jag studerat malariamyggor i laboratorium och fält, och kartlagt deras rörelsemönster flera dagar i sträck. Därmed framkom att hanmyggor svärmar på specifika platser vid exakt samma tidpunkt varje kväll, och att honmyggor konsekvent flyger in till befolkade områden i jakt på blod i samband med solnedgången.

Mät- och analysmetoderna har nu nått en brytpunkt där de kan appliceras på faktiska biologiska frågeställningar. I samband med att tekniken och kompetensen sprids, och att förståelsen för insekters optiska egenskaper ökar, finns det möjligheter att rädda människoliv genom kartläggning av smittobärande insekter, att bekämpa skadedjur mer effektivt för att reducera användandet av pesticider, och att förbättra förståelsen för ekosystemen runt omkring oss och deras växelverkan med vårt samhälle.

Abstract

This thesis treats entomological lidar from various angles: laboratory reference work on insects of interest, methodological development of lidar- and data processing methods, as well as field implementations of lidar techniques for entomological research. Insects are crucial components of ecosystems and are currently in a global decline. In this thesis, insects are mainly studied in their roles as disease vectors and food sources for vertebrates. However, several other feasible application avenues of entomological lidar exist and are touched upon briefly. Entomological lidar is an optical remote sensing technique in which the light scattered by insects is recorded by a sensor and the distance to each insect is derived. In classical lidar, ranging is achieved through time-of-flight detection. In this thesis the Scheimpflug- and passive lidar methods have been used, in which ranging is achieved through triangulation and geometrical optics.

In the laboratory reference work, the light-scattering properties of insects were investigated. Considerable effort has been put into the study of *ex-vivo* and *in-vivo* malaria mosquitoes in search of optical properties that may enable remote species classification. These species otherwise require capture and microscope analysis by an expert to distinguish. Dragonflies have the narrowest spectral bands so far observed in nature. In this PhD work, their scattering properties were investigated and give hints regarding possible uses of these narrow bands.

Methodological development has been pursued for improvement and optimization of instrumentation through simulation and laboratory reference measurements. Hyperspectral images of insects were used to motivate laser wavelength selection based on signal strength, information yield and laser availability. Raytracing was used to devise a passive lidar scheme and to optimise the geometry of Scheimpflug lidars. Data processing techniques for robust and accurate calibration of sizes, wing-beat frequencies with associated modulation spectra, flight headings and dispersal of insects in lidar data were developed.

Entomological lidar techniques were applied in a number of field settings around the world. In Sweden, insect swarms at the nacelle of a wind farm were observed post sunset in weather conditions associated with high bat mortality through collision with wind farms. In China, increased insect activity was observed at the onset of heavy rain. The main crepuscular activity peak of insects was observed in the short time window with decreased predation pressure around sunset, when

neither birds nor bats were active. In Africa, an extra activity peak was observed at noon among mosquitoes and other crepuscular insects during a solar eclipse. Male mosquito mating swarms were observed with consistent timing and location each day, and a highly directional dispersal of mosquitoes into a village was observed every evening.

In this thesis work, peak numbers of more than a thousand insects per minute have been observed, resolved temporally and spatially at μs and cm scales, respectively, which is inconceivable with conventional entomological methods. Laboratory reference work and methodological development allow the quantification and classification of insect signals *in-situ*. Thereby, questions of significant ecological importance could be answered.

1. Introduction

We see, we hear, and we smell. While writing this thesis, I can see the pigeon on the windowsill, I can hear the traffic on the street outside, and I can smell the coffee brewing in the kitchen. We are born with these senses, and through experience we learn to use them intuitively in order to understand our surroundings from a distance. This is the fundamental principle of remote sensing – using our senses to acquire information remotely. Oftentimes, this is done with so-called passive remote sensing, in which the signal carrying information about an object has an external origin. The signal source may be the ambient light which is scattered by the pigeon, the sound produced by the car engines, or the coffee particles themselves travelling through the air by diffusion. In passive remote sensing, the observer has no control over the signal source. Active remote sensing, in contrast, makes use of an internal, or controlled, signal source. This may correspond to using a flashlight to navigate a dark room or to dropping a rock into a well to determine its depth. Through technological development, our ability to make sense of our surroundings from a distance has improved significantly.

1.1. Optical remote sensing

Optical remote sensing methods utilize light to gain information about a target remotely. These methods are used in a wide range of industries and activities, including topographic mapping [1], forest characterization [2], autonomous vehicle research [3] and mapping of aerosols [4, 5] and gases [6, 7] in the atmosphere. Light detection and ranging (lidar) is a technique that was developed during the second world war using search lights [8]. Since then, lidar techniques have developed to make use of powerful lasers for improved sensitivity. In the past fifteen years [9, 10], optical sensing techniques have been developed for ecological applications, resulting in lidar systems specialized for insect detection [11-13], automated electronic insect traps [14] and inelastic hyperspectral aquatic lidar [15]. Furthermore, optical techniques for distinguishing salmon lice from other zooplankton in salmon farms are being developed [16].

In entomological lidar, lidar technology is adapted for efficiently studying insects. Thus, the disciplines of atmospheric optical remote sensing [7], in which lidar is employed to monitor gases and aerosols in the atmosphere [4, 6], and biophotonics, in which the optical properties of biological tissue are investigated and utilized in medical applications [17-19], are merged. Fast acquisition allows

retreival of wing-beat frequencies, which relate to the species, sex and payload of an insect, and the spectral contents of a signal may yield information on wing thickness and the water- and melanin contents. Polarization properties [9] can be used to distinguish between matte and glossy wings, relate to species and sex and have even been shown to enable distinction of gravid and non-gravid female mosquitoes [20].

1.2. Other remote sensing domains

1.2.1. Radar

Radar is a tool that has been utilized in ecology for more than 40 years [21]. There are dedicated systems used in entomology [22] and ornithology [23, 24], as well as extensive networks of weather radars which may be utilized for ecological studies [25-27]. Entomological radar systems can be used to estimate the activity and flux of insects. The potential for target classification has been demonstrated [28], utilizing the radar cross section (RCS) and other signal parameters. Wing-beat frequencies (WBF) of insects are generally not observable in radar signals due to the wings being dry, and the RCS largely originating from the water contents in

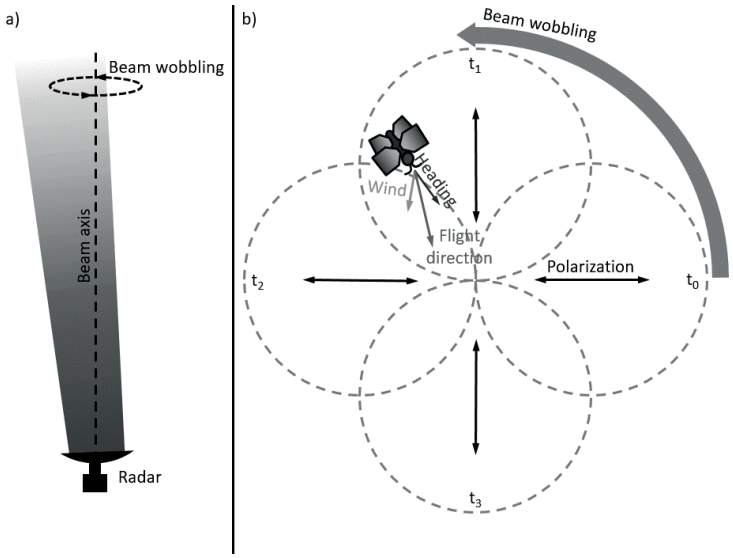

Figure 1.1 Heading and flight direction in entomological radar. *By wobbling the beam and rotating the polarization, the heading and flight direction of aerofauna flying through the beam is obtained.* ***a****) The radar beam is transmitted vertically into the air. By angling and rotating the radar antenna, the beam is wobbled around its own axis.* ***b****) An insect flying through the wobbling beam. The flight direction is obtained through the beam wobbling, and the heading angle/orientation of the insect is obtained from the rotating polarization.*

insect bodies. Rotating the polarization of the transmitted beam yields an oscillating RCS, enabling deduction of the heading of an insect flying through the beam [28], see Figure 1.1. In addition, by wobbling the beam, the flight direction can be determined [29]. Radar systems are generally robust and may be deployed and run without supervision for long periods of time. Many radar systems have a near limit for detection of about 200 m and may only be deployed vertically due to ground clutter. The theoretical capability of two entomological radar systems to detect a few insect species of interest is shown in Figure 1.2. Passive coherent location (PCL) radar [30] makes use of third party transmission of microwaves, e.g. FM radio, and phased array antennae to deduce the location of a moving object. However, the method suffers from low signal-to-noise ratios (SNR), and insect detection with PCL radar is unfeasible.

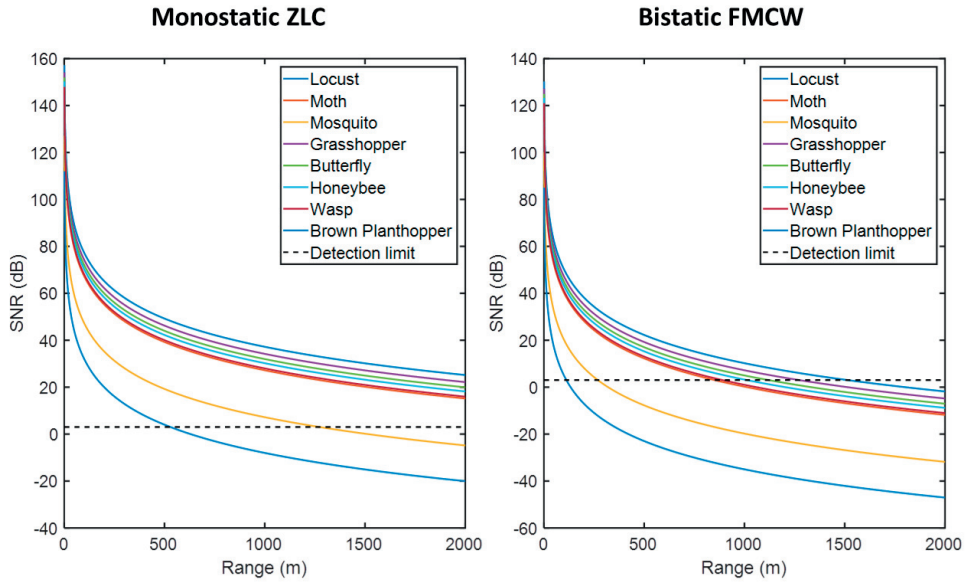

Figure 1.2 Estimated signal-to-noise ratios of two radar designs for a number of entomological target species. *Two theoretical entomological radar systems were designed and evaluated: a monostatic zenith-pointing linearly-polarized conical scan radar (ZLC) and a bistatic frequency-modulated continuous wave radar (FMCW). The signal-to-noise ratios (SNR) of different insect targets for both systems were evaluated based on the distance between the radar system and the target. Although the ZLC radar is able to detect insects further away compared to the FMCW radar, it comes with drawbacks such as being blind at close range (~200 m). Both types of systems are used in research on animal migration [22, 31].*

1.2.2. Acoustics

Sound-based remote sensing has been used underwater since 1906, when the first

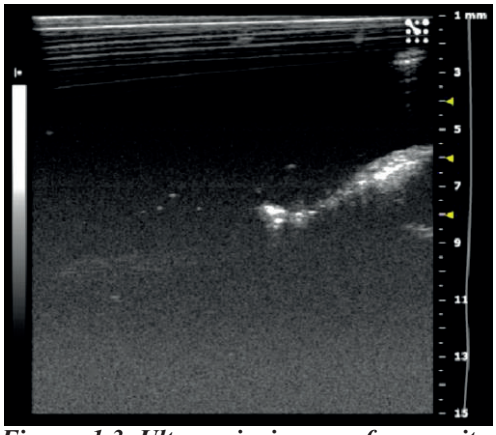

Figure 1.3 Ultrasonic image of mosquito larva. *Ultrasonic waves have been proposed as a method of killing mosquito larvae in water to benefit integrated vector management programs without resorting to usage of chemicals [32].*

sound navigation and ranging (sonar) device was invented by Lewis Nixon to detect icebergs. Since its conception, implementations of sonar have been used for both military and civilian purposes, in particular in the fishing industry [33]. Ultrasound (Figure 1.3) is a diagnostics tool in medicine, used to image tissue inside the body [34]. One of the most common applications is examination of unborn babies inside the womb of their mothers. In ecology, ultrasonic sensors are commonly used to detect the sound pulses transmitted by bats for echolocation (Figure 1.4), and ultrasonic transducers have been used in attempts to deter bats from dangerous locations [35]. Bioacoustic methods have been used to assess biodiversity, and computational bioacoustics makes use of sound for species classification [36, 37]. With passive acoustic

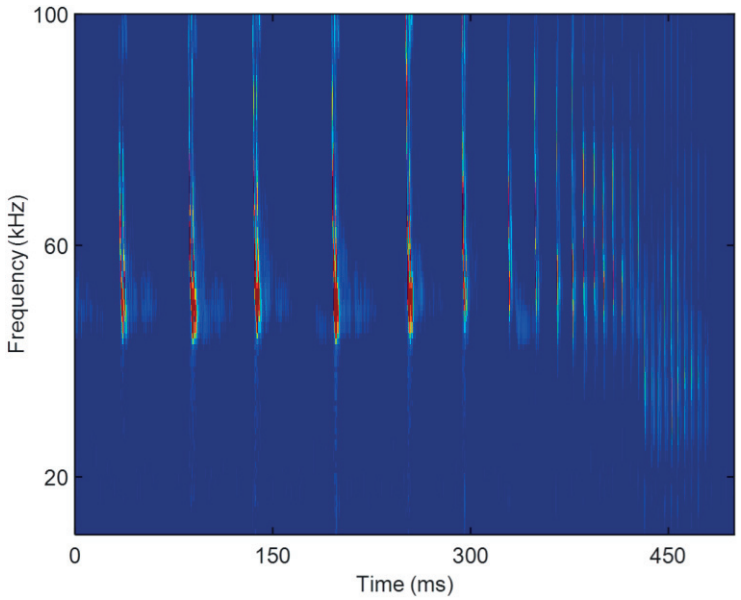

Figure 1.4 Search calls and a feeding buzz from a common pipistrelle (Pipistrellus pipistrellus) hunting insects at night. *Bats use echolocation to find and trace insects. They transmit pulses faster and faster as they approach their prey, ending with a low-frequency "feeding buzz" as they finally catch and devour it.*

detection, localization has been made possible through the implementation of sound phase arrays, where the positions of birds are determined by the time their calls arrive to different array elements [38]. Recently, acoustic sensors for detecting and classifying species and sexes of mosquitoes have been demonstrated [39], and methods using the microphones of regular cell phones are being developed for crowd-sourced mosquito detection [40].

1.3. Entomological overview

1.3.1. Field-sampling methods

Insects have been studied for a long time, resulting in the development of a large number of investigation methods. Conventional methods typically rely on catching the insects [41] and include the usage of sweep nets [42] and elaborate traps, which attract insects in different ways using e.g. pheromones [43], CO_2 [44] or light [45]. In a recent study, migrating mosquitoes were caught a few hundred meters above ground with sticky tape attached to balloons [46]. These methods (Figure 1.5) require a lot of manual labor and yield comparatively low numbers of insects compared to remote sensing techniques. By necessity, they employ low time resolution on a scale of hours or even days. Certain flight parameters, such as exact timing and flight direction, are difficult to measure. In addition, traps and other catch-based methods are known to have systematic biases and may attract different insect species, sexes and age groups to different extents. Despite these

Figure 1.5 Mosquito traps in Lupiro, Tanzania. a) *Experimental huts where humans lie as mosquito bait at night. Female mosquitoes enter the huts in search of a blood meal, and their bite timing and subsequent behavior is studied.* ***b)*** *Trap used to catch mosquitoes. Photos by Samuel Jansson.*

drawbacks, sampling methods may yield rich information on each individual insect obtained. Genetic sequencing [47], microscopic evaluation [48], mass spectroscopy [49] and chromatography [50] can provide information on sexual maturity, dietary choices of individuals, relatedness of populations, and much more.

1.3.2. Disease vectors

One entomological lidar application is disease vector monitoring. Malaria, which is spread by mosquitoes (Figure 1.6), claims close to half a million lives each year and has severe economic consequences for some of the poorest countries in the world [51-53]. Including all warfare, terrorism and crime, humans are still left in second place as mosquitoes are the world's most lethal animals. Apart from malaria, mosquitoes spread other illnesses such as dengue fever, the zika virus and yellow fever, which may have fatal outcomes at times. Mosquito species that specialize in feeding upon humans are very efficient vectors of malaria, and affect rural areas in the African countryside disproportionately [54, 55]. The implementation of vector control with insecticide-treated bed nets and indoor residual spraying has reduced the malaria burden significantly since the turn of the century [56, 57]. However, mosquitoes have adapted their biting hours as a result [58]. Progress has stalled [59], and further reduction of the malaria burden necessitates improved understanding of mosquito behavior [60].

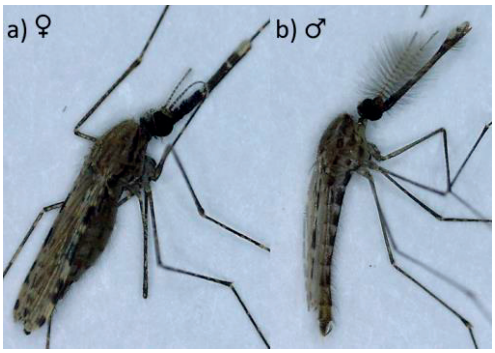

Figure 1.6 Microscopic images of Anopheles arabiensis mosquitoes. *Anopheles arabiensis is one of the main malaria vectors in large parts of Africa. a) Female An. arabiensis mosquito, characterized by a slightly larger abdomen with a blood sac and a needle with which to penetrate skin. Females are attracted to human hosts by the carbon dioxide we exhale, and ingest blood to develop fertile eggs. b) Male An. arabiensis mosquito, characterized by its furry antennae. Photos by Mikkel Brydegaard.*

1.3.3. Pests

Insect pests cause significant damage in forestry and agriculture. Pests are one of the primary causes for the reduction of crop yield, and cause an annual loss of up to 10% of the production [61]. They are a major plague in forestry, causing up to

60% of tree deaths [62]. Bark beetles (Figure 1.7) are the most prevalent forestry pest, and outbreaks often follow storms [63] and wildfires [64]. The damage caused by pests prompts large-scale usage of pesticides and insecticides, which in turn can have severe consequences for human health [65]. The overuse of

Figure 1.7 Bark beetles preparing for take-off. *Bark beetles are a major pest in forestry, causing a large amount of tree deaths. They normally do not attack healthy trees – however, when large amounts of trees have been felled by a storm or wildfire it may lead to an outbreak during which the number of beetles increases to such a level that even healthy forest is affected.* ***a)*** *Bark beetles poised for take-off in Nyteboda forest in southern Sweden. The area was hit by a storm a few years ago, and suffers from seasonal pest outbreaks since then. Photo by Mikkel Brydegaard.* ***b)*** *A captured bark beetle with wings extended. Photo by Meng Li.*

pesticides can have additional adverse effects, improving the flight capacity of long-distance migratory recurrent pests [66] and causing outbreaks by increasing the fecundity of insects [67, 68]. Automated insect monitoring in agricultural- and forestry settings may predict pest outbreaks [69], thereby reducing the need for continuous application of pesticides.

1.3.4. Pollinators

Pollinators provide important services to most terrestrial ecosystems, wild [70] or cultivated [71]. Bees in particular are the main pollinators of most crops, and are crucial for sustainable agriculture. As such, the currently observed decline of pollinators may have severe economic consequences, and significant negative impact on biodiversity [72] and human nutrition and health globally [73]. The pollinator decline has been shown to depend on a number of factors, such as habitat loss [74], the introduction of foreign species, climate change [72] and pesticide usage [75].

1.3.5. Migrants

Animal migration involves a massive displacement of biomass covering the entire planet [76]. Many animals migrate, including e.g. birds [77], moths (Figure 1.8) [78, 79] and mosquitoes [46]. The same species may form an integral part of two or more distant ecologies [77] and may carry diseases and parasites between different habitats [80]. Migration is strongly affected by climate change [81], and some populations are declining [82]. Improved monitoring tools are crucial for improving our understanding of these phenomena and to aid in mitigation efforts.

Figure 1.8 Bogong moths aestivating on cave walls after migration flight. *Bogong moths have a peculiar life cycle. They hatch in winter all over south-eastern Australia and migrate up to 965 km to spend the summer months aestivating on cave walls in the Australian Alps [83]. Upon reawakening, they migrate once more, back to their birthplace where they mate and die, restarting the cycle. Photo by Anna Honkanen.*

1.3.6. Prey insects

Insects constitute food sources for many species of vertebrates, including birds such as swifts and swallows [84, 85] and bats (Figure 1.9). Bats comprise many protected species that are endangered by human activities. This is effected by urban expansion, increasing light pollution [86] and wind power production [87, 88], among other things. Wind farms alone account for an estimated loss of several hundred thousand bats each year in Europe and North America [89-91]. Through the study of prey insects, insights regarding the behavior of insectivores may be obtained to reduce the number of deaths.

Figure 1.9 P. pipistrellus bats foraging in a manure well near a wind farm in Östra Herrestad, Sweden. *Dung and manure are well known to attract large amounts of insects. Large collections, such as the wells used by farmers to produce manure for their fields, are therefore excellent hunting grounds for bats. Photo by Jens Rydell.*

2. Light and light-insect interaction

2.1. Light descriptions

Light is an essential part of existence and defines our diurnal rhythm through the day-night cycle, which is a fundament of our society. By segmenting the day into periods of light and dark, of hot and cold, animals evolve and adapt their behavior to improve their chances of survival and reproduction [92]. Thereby, interaction dynamics emerge, forming complex ecosystems in which predators and prey compete [93]. Despite being so fundamental to our lives, light is a complex phenomenon that has been studied considerably. Its interaction with matter is a subject of further study. Light can be understood or interpreted in different ways, some of which are described below.

2.1.1. Rays

The description of light as rays is the earliest [94] and simplest treatment, and has been used to design ground-breaking optical instruments through the ages, such as the telescope [95]. In ray optics, light is treated as rays travelling from a light source to an observer. The refractive index n describes how light propagates through a medium, and the speed of light through the medium is given by $c=c_0/n$, where c_0=299792458 m/s is the speed of light in vacuum. Modern day developments of computational power have led to the rise of raytracing, in which large numbers of rays are simulated in complex optical systems (used in Paper V). However, ray-optical models are inefficient for describing many properties of light, such as interference, diffraction or propagation in turbid media, for which wave optics is required.

2.1.2. Waves

The wave theory of light was established by Thomas Young in the beginning of the 19th century and demonstrated in the famous double slit experiment [96]. Wave optics encompasses ray optics, but offers explanations for phenomena like interference, diffraction, Mie scattering, polarization of light, spatial frequencies and structural colors. The complex wavefunction, $U(r,t)$, describes a light wave in time and space, where $r=(x,y,z)$ describes a location in space and t denotes the time. Any function $U(r,t)$ that satisfies the wave equation, Equation (2.1), is a possible optical wave.

$$\nabla^2 U - \frac{1}{c^2}\frac{\delta^2 U}{\delta t^2} = 0 \quad \textbf{(2.1)}$$

The spherical wave, Equation (2.2), is a solution to the wave equation of particular importance. By superimposing spherical waves (Figure 2.1), approximate solutions to components such as gratings can be obtained.

$$U = \frac{U_0}{r} \mathrm{e}^{-i2\pi r/\lambda} \quad \textbf{(2.2)}$$

In Equation (2.2), U_0 is the light strength at the source and λ is the wavelength.

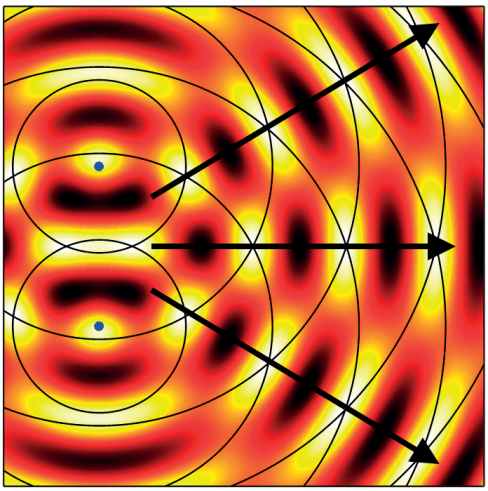

Figure 2.1 Interference of point sources. *Two point sources (blue dots) interfere with each other, producing an interference pattern. The wave fronts from both point sources are marked with black lines. Constructive interference is observed in areas where wave fronts overlap.*

2.1.3. Photons

The photon interpretation of light treats it as a collection of elementary particles called photons. The photon is the quantum of the electromagnetic field, and is described as a massless particle with an impulse [97, 98]. The intensity I of light is proportional to the photon density, and particles have interaction cross sections, or probabilities, μ, of interacting with photons, which govern light transport in dense or turbid media. For example, the scattering coefficient μ_s relates to the photon being scattered by a particle, and the absorption coefficient μ_a relates to the photon being absorbed.

2.1.4. Light properties

Light from any given light source has a number of properties. The intensity of light corresponds to the square of the electric field amplitude in vacuum. The light intensity from a point source given by Equation (2.2) condenses into Equation (2.3). Light intensity is normally measured in units of W/m^2.

$$I = U^2 = \frac{U_0^2}{r^2}|\mathrm{e}^{-ikr}|^2 = \frac{U_0^2}{r^2} = \frac{I_0}{r^2} \quad \textbf{(2.3)}$$

Light has a frequency f which relates to the photon energy in the photon interpretation, and to the oscillation frequency of the electric field in the wave interpretation. The energy of a photon is given by Equation (2.4), in which h is Planck's constant, f is the oscillation frequency and λ is the wavelength in vacuum.

$$E_{phot} = hf = \frac{hc_0}{\lambda} \tag{2.4}$$

As the light amplitude undergoes periodic oscillations, the stage of the oscillation at which the light is at any given time is called phase. In optics, the absolute phase of a wave cannot be acquired. However, the relative phase or phase difference between two waves may be measured with interferometric techniques, e.g. Doppler lidar [99] and optical coherence tomography [100].

The polarization direction of light corresponds to the oscillation direction of the transverse electric field component in the wave interpretation. Light may contain multiple polarizations simultaneously, and the complete polarization of light is described by the four parameters in the Stokes vector [101]. For light impinging on a surface, the polarization is described in terms of s- and p-polarization, where s-polarized light is polarized perpendicular to the plane of incidence, and p-polarized light is polarized parallel to the plane of incidence. This description is used in Paper IV. In radar application, the notation HH, VV, HV and VH is used, wherein H and V correspond to horizontal and vertical polarization. The first letter in each combination corresponds to the transmitted polarization, and the second letter corresponds to the received polarization. In biophotonics, the polarization of light is described by the terms co-polarization and depolarization [101], which is used in Paper I-III, VI-VII, IX and XI. For linearly polarized light, the oscillations of the electric field occur in one direction only. Unpolarized light has random polarization. Other polarizations include elliptical polarization, in which the two polarization components have different phase. In that case, the polarization direction rotates periodically around the optical axis. The reflection from some scarab beetles has been shown to be elliptically polarized [102]. Certain materials and structures interact differently with light depending on its polarization. Polarizers, for example, selectively absorb light with polarization along one axis, while fully transmitting light with the other polarization. Birefringent crystals have different refractive indices in different spatial directions, thereby affecting the two polarization components differently. The degree of linear polarization (DoLP) corresponds to the fraction of light that maintains its polarization through the interaction with a sample and is calculated according to Equation (2.5). Linearly polarized light has a DoLP=1, whereas fully depolarized light has a DoLP=½.

$$DoLP = \frac{I_{co}}{I_{co} + I_{de}} \tag{2.5}$$

Interaction processes between light and matter can generally be divided into coherent interaction, wherein the polarization, phase and propagation direction of

the light is preserved, and incoherent interaction, wherein the light loses its polarization.

2.2. Coherent interaction processes

Light sources and interaction processes can be divided into two categories: coherent and incoherent. Coherent light sources, such as lasers, produce light in which the photons are in phase, whereas incoherent light sources produce light with random phase. Similarly, coherent interaction processes are processes in which the phase of light is preserved, whereas incoherent interaction may change the phase of light.

2.2.1. Refraction

Light changes propagation direction when passing from one medium to another, an effect called refraction (Figure 2.2). The refraction angle θ_2 depends on the incident angle θ_1, as well as the refractive indices of the two mediums, n_1 and n_2, according to Snell's law, see Equation (2.6). Some refractive indices of relevance to this work are melanin with n=2.5, water with n=1.3, chitin with n=1.5 and biological tissue in which n is proportional to the density [17]. Air has a refractive index n=1.

$$n_1 \sin\theta_1 = n_2 \sin\theta_2 \tag{2.6}$$

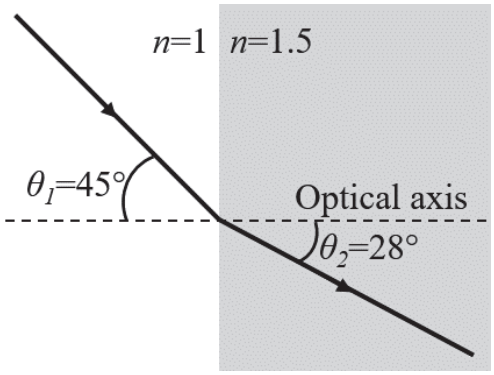

Figure 2.2 Refraction of light. *As a ray of light transitions from one medium to another, the change in refractive index effects a change in the direction of propagation. Since the speed of light in a medium is inversely proportional to the refractive index, refraction can also be expressed as light taking the shortest optical path between two points (Fermat's principle).*

Furthermore, the transition of light between two mediums results in some of the light being transmitted through the surface between the mediums, and some of the light being reflected. The amount of light that is reflected and transmitted depends on the polarization of the incident light, according to the power reflectance and transmittance described by Fresnel's equations, Equation (2.7), and relate to Paper IV. These equations are derived for flat surfaces, whereas many insects have wrinkled wings which reduce the reflectance and may reduce predation risk [103, 104].

$$R_s = \left|\frac{n_1 \cos\theta_1 - n_2 \cos\theta_2}{n_1 \cos\theta_1 + n_2 \cos\theta_2}\right|^2, \quad T_s = 1 - R_s,$$
$$R_p = \left|\frac{n_1 \cos\theta_2 - n_2 \cos\theta_1}{n_1 \cos\theta_2 + n_2 \cos\theta_1}\right|^2, \quad T_p = 1 - R_p, \tag{2.7}$$

where R_s and T_s are the reflection and transmission coefficients for light with a perpendicular polarization to the plane of incidence, and R_p and T_p are the coefficients for light with a parallel polarization to the plane of incidence. There exists an angle at which the reflection coefficient for light with parallel polarization to the plane of incidence is zero (Figure 2.3), called the Brewster angle θ_B. The Brewster angle is described by Equation (2.8).

$$\theta_B = \tan^{-1}(n_2/n_1) \tag{2.8}$$

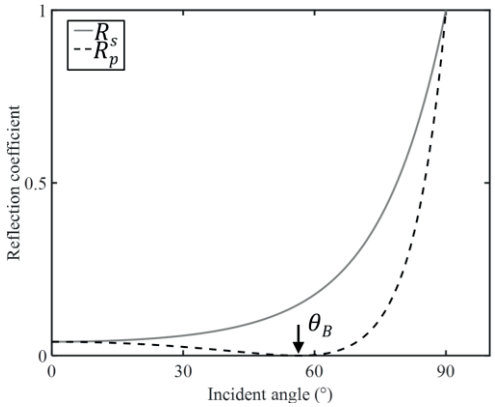

Figure 2.3 Reflection coefficients an air-chitin transition (n_1=1, n_2=1.5). *Light with different polarizations are reflected to different extents when impinging on a surface. The reflectance coefficient is zero for p-polarized light impinging at the Brewster angle. In the air-chitin transition, this occurs at 56°.*

An important outcome of Snell's law of refraction, and one that has been utilized heavily in this PhD work, is the lens equation. When an object is placed adjacent to a lens outside of the focal point, an image of the object is formed on the opposite side of the lens (Figure 2.4). The imaging properties of a lens are described by its focal length f and aperture Ø. The distances between the object and the lens, z_1, and between the lens and the image, z_2, are related according to Equation (2.9), and the magnification M of the lens is given by Equation (2.10). Furthermore, the amount of light collected by a lens is proportional to the square of the aperture, $Ø^2$, and the

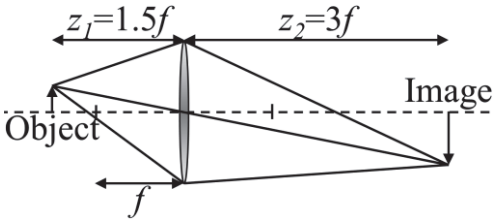

Figure 2.4 Image formation by a lens. *When an object is place next to a lens, an image is formed on the other side. The effect is reciprocal. As the object moves closer to the focal point of the lens, the image moves towards infinity. If the object is a sensor, focus is obtained at different distances by adjusting the distance between the sensor and the lens.*

angular resolution relating to the point spread function is proportional to λ/Ø, where λ is the wavelength of light. Therefore, a large aperture is crucial for retrieving backscatter at a fast pace from small point sources such as insects in e.g. Scheimpflug lidar.

$$\frac{1}{f} = \frac{1}{z_1} + \frac{1}{z_2} \tag{2.9}$$

$$M = -\frac{z_2}{z_1} \tag{2.10}$$

2.2.2. Single scattering

Single scattering is a phenomenon in which light changes its direction of propagation through the interaction with a particle or object. The direction change is described by a phase function, which indicates the amount of scattered light in each direction. Three scattering regimes are defined, based on the size of the particle or object: geometrical optics, Mie scattering and Rayleigh scattering. Geometrical optical theory, such as refraction which is described in Chapter 2.2.1, sufficiently describes the processes that occur when the particle or object is significantly larger than the wavelength of the light. Rayleigh scattering describes the process when the scattering particle is significantly smaller than the wavelength of light, as is the case with atoms and molecules in the atmosphere [105]. The Rayleigh scattering cross section is proportional to λ^{-4}, indicating that light with shorter wavelengths are significantly more probable to scatter than light with longer wavelengths. Mie scattering describes the scattering process when the size of the scattering particle is roughly the same as the wavelength of the light [106, 107], and has a scattering coefficient with an approximate λ^{-2} dependence, where the exponent depends on the particle size [108]. Mie theory is typically used to describe the interaction of light with spherical aerosols in the atmosphere, and Mie phase functions are complex and contain angular scattering lobes. The Henyey-Greenstein phase function is a simplified description that does not contain scattering lobes, and is described in Equation (2.11). By changing one parameter, called the anisotropy coefficient g ($-1<g<1$), scattering goes from backscattering, through isotropic scattering, to forward scattering. The phase functions obtained from a mosquito through goniometry in Paper I correspond approximately to the Henyey-Greenstein phase function. Paper I further illustrates that ballistic light and single scattering are dominant in tiny insects such as mosquitoes, compared to multiple scattering.

$$p(\theta_{sc}) = \frac{1}{4\pi} \frac{1 - g^2}{(1 + g^2 - 2g\cos(\theta_{sc}))^{3/2}} \tag{2.11}$$

in which θ_{sc} is the scattering angle and p is the probability.

2.2.3. Interference

Interference is a process in which two or more light waves with different phase interact with each other, producing a new wave which is a superposition of the original waves. Light from the same light source may interfere with itself after travelling along different paths.

When light impinges on a thin film, interference occurs at the back- and front side of the film. Depending on the thickness of the film, the interference may be either constructive or destructive, which determines how much light is transmitted and how much is reflected. Thin-film interference is a prominent feature in light reflected in insect wings (Figure 2.5) [109]. One-, two- and three dimensional structures of spatial frequencies may also cause light to interfere with itself. The grating is a basic optical component in which this occurs, but there are many examples in nature as well [110, 111]. Volumes exhibiting dominant spatial frequencies may produce so-called structural colors, which can be spectacular [112, 113] and account for the darkest [114] colors so far observed in nature. Iridescence is another structural phenomenon in which the color of an object or animal depends on the angle from which it is observed [115, 116].

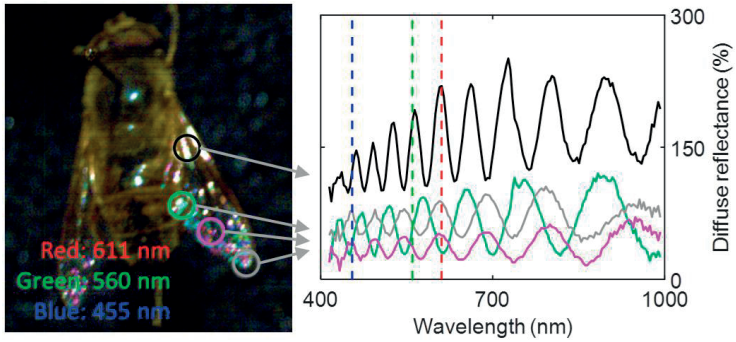

Figure 2.5 Thin film interference in the wing of a fly. *The reflectance is compared to a diffuse target, and specular reflexes may therefore reach several hundred percent reflectance. Depending on the wavelength, light may interfere in the back- or forward scatter direction, resulting in spectral fringes. The reflexes appear colored when constructive interference is obtained in one or two visual bands and bright white when it is obtained in all visual bands simultaneously, which is normally the case in human vision due to our broad spectral bands. The separation of fringes is spectrally shorter at the root of the wing where the membrane is thick, and spectrally longer at the tip of the wing where the membrane is thin. This is consistent with how the free spectral range of a Fabry-Perot interferometer changes with membrane thickness. The image was acquired with a hyperspectral camera.*

2.3. Incoherent interaction processes

2.3.1. Absorption

When light is propagating through a medium, the energy is absorbed and converted into other energy forms, most often thermal energy, with a certain probability per unit length. This is modelled by the Beer-Lambert law, Equation (2.12), in which the intensity of transmitted light I is calculated based on the original intensity I_0, the absorption coefficient μ_a and the distance l travelled through a medium.

$$I = I_0 e^{-\mu_a l} \tag{2.12}$$

The absorption coefficient further relates to the refractive index of a medium through the Kramers-Kronig relations [117]. In addition, the absorption coefficient (and consequently the refractive index) is wavelength-dependent. Absorption occurs when the wavelength, i.e. photon energy, corresponds to the transition energy of an atom or molecule. For visible light, this typically corresponds to the excitation energies of electrons in the outer shells, whereas infrared wavelengths correspond to vibrational transitions. Chitin [118] and keratin [119] have absorption peaks in the ultraviolet (UV) region, around 280 nm. Melanin [120] exhibits a gradually decreasing absorbance with longer visible wavelengths, resulting in a brown color. The absorption coefficient of melanin can be described as $\mu_a = C\lambda^{-3.48}$, where C is a constant [121]. Water exhibits absorption peaks in the short-wave infrared (SWIR) region. Many spectral features of insects can be described well by the absorbance of melanin and water (Figure 2.6). The melanisation is used in Paper II to distinguish between *An. coluzzii* and *An. arabiensis* mosquitoes.

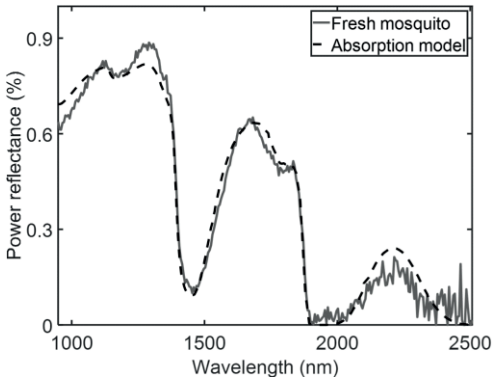

Figure 2.6 Absorption in fresh mosquito sample. *The reflectance spectrum of a fresh mosquito was obtained from a hyperspectral image. A model containing the absorption coefficients of water and melanin corresponds well to the mosquito spectrum. The model used an equivalent water path length of 700 μm.*

2.3.2. Multiple scattering

In dense and turbid media such as tissue [17], light is usually scattered multiple times. In that case, any coherence the light may have had before entering the scattering medium is lost, as photons travel different paths and are scattered a

different number of times before exiting the medium. The whitest color observed in nature corresponds to a very high scattering coefficient [122]. Multiple scattering may also be referred to as photon migration or diffuse scattering [123], and lacks the directionality of specular scattering. This anisotropy may be modeled by the Henyey-Greenstein phase function, see Equation (2.11). An ideal diffusely scattering surface is called a Lambertian, and scatters equally in all directions. Multiple scattering is often simulated with Monte Carlo simulations, in which the scattering properties of a medium are defined, and billions of simulated photons are sent into the medium to determine the scattered light distribution [124, 125]. When light propagates through a medium a certain amount loses its direction of propagation through scattering of absorption. This is referred to as extinction, and is utilized in Paper I-II.

2.3.3. Depolarization

Light travelling through a sample may lose its polarization state in a process called depolarization [126]. When light is scattered in a particle there is a chance for it to lose its polarization based on the geometrical and physical characteristics of the particle. As the light undergoes multiple scattering events the likelihood of deviations from the original polarization state increases. For linear polarization, the rate of depolarization per unit length in a sample is determined by the depolarization coefficient μ_{LP} [101]. Thereby, the DoLP of scattered light, obtained according to Equation (2.5), may shed light on the optical properties of a sample through Equation (2.13). Should the optical path length in the sample be known, μ_{LP} may be inferred.

$$DoLP = {}^{1}/_{2} + {}^{1}/_{2}\, e^{-\mu_{lp} l} \tag{2.13}$$

The depolarization ratio has been demonstrated as a parameter that can be used to distinguish gravid and non-gravid mosquitoes [20], and is used in Paper IX to distinguish insects from rain drops.

2.4. Dynamic properties

Optical signals obtained from insects normally contain both coherent and incoherent parts, corresponding to scattering in different parts of insect bodies (Figure 2.7). These signals are varying periodically in time as insects beat their wings. Decoupling these signal contributions is a complex process that is explored in Chapter 4. The different signal components contribute to different features in the frequency domain. The body scatter is static and contributes only to the lower end of the frequency spectrum. The wing scatter has an incoherent (or diffuse) part which contributes to the wing-beat frequency and the first few overtones. The coherent wing scatter appears in the form of sharp specular spikes as the wing membrane reflects light straight into the sensor. These spikes have a very short duration in time, and contribute to high overtones in the spectrum. Accordingly, up

to 27 overtones have been observed from fruit flies in a laboratory setting, as shown in Paper IV. The dynamic properties of insects are further explored in Paper II-XIII.

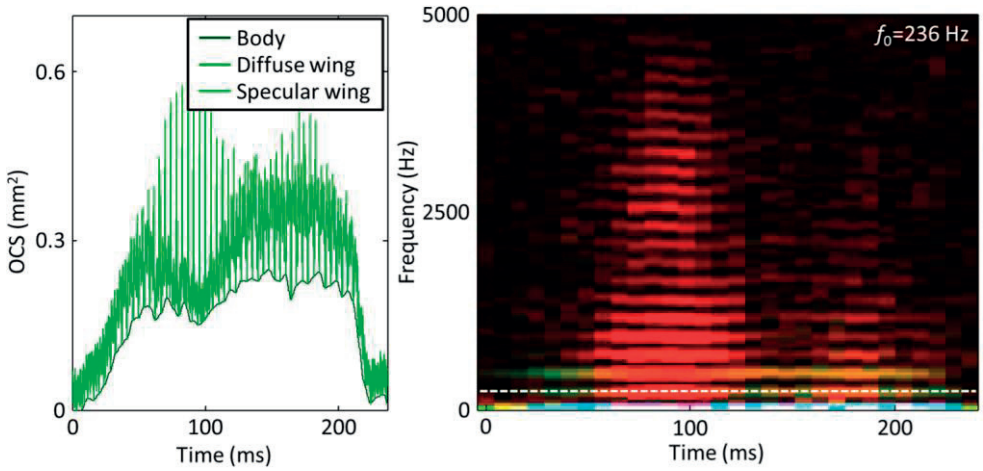

Figure 2.7 Coherent and incoherent dynamic signal contributions from a fruit fly, Dr. melanogaster. Left*) The time-series signal is separated into three components: body-, diffuse wing- and specular wing scattering. The wing scatter appears mostly diffuse, however a series of specular reflections are observed between 60 and 120 ms.* ***Right****) False-color image of the spectrograms of the three signal components. The body spectrogram is shown in blue, and only contributes to the lower frequencies. The diffuse wing spectrogram, shown in green, contributes mainly to the first two harmonics. A burst of higher harmonics appears in the specular wing spectrogram, shown in red, due to the specular spikes in the time series.*

3. Instrumentation

3.1. Light sources

3.1.1. Ambient light

Ambient light is used extensively in remote sensing. Lunar obscuration is a conventional method for studying nocturnal bird migration [127]. The Sun is a readily available light source that can be utilized in a variety of passive optical detection schemes, e.g. Paper V and [128, 129], and by aiming a setup towards the Polaris star the incident sunlight on the field of view (FoV) is always approximately 90º [130]. The Sun is a strong light source with a broadband spectrum which can be approximated as blackbody radiation with the solar surface temperature of 5778 K. It has its emission peak in the green wavelength regime, at around 500 nm. Due to absorption in the atmosphere, some solar wavelengths do not reach the surface of the Earth. Narrow absorption lines from the UV to the near infrared (NIR) regions are called Fraunhofer lines, and correspond to specific atomic transitions. Broader absorbed spectral regions are found in the mid-infrared (MIR) region, corresponding to vibrational or rotational molecular transitions. Measurements using the Sun as light source are restricted to daytime usage, and require a clear sky. They are therefore unsuitable for studying crepuscular or nocturnal phenomena.

3.1.2. Light emitting diodes

A light emitting diode (LED) is a semiconductor light source [131]. It consists of a so-called p-n junction, which is the interface between two semiconductors. One of them is n-doped (negative), indicating that it contains an excess of electrons, and the other is p-doped (positive), indicating that it contains an excess of electron holes. There is a difference in electric potential, called bandgap, between electrons in the conduction band and holes in the valence band. Thus, applying a voltage to the p-n junction (p-doped to anode and n-doped to cathode) causes electrons to fall across the bandgap to the lower potential and recombining with holes in the p-doped material, thereby generating a current across the p-n junction. The recombination process generates emission of photons with an energy and wavelength equivalent to the bandgap of the material, and a stronger voltage yields a higher light intensity. Light is emitted in a semi-random direction, with random

phase and polarization. LEDs are inexpensive and available commercially in a large range of wavelengths. Requiring only low voltage and current to run, LEDs are simple and robust light sources that are suitable for many studies, such as Paper I and VII in this thesis.

3.1.3. Laser diodes

Light amplification by stimulated emission of radiation (laser) is a phenomenon in which coherent light is produced. Though many laser sources exist, multimode laser diodes (LDs) have been used exclusively in this PhD work. Compared to other laser sources, they benefit from low cost, complexity, weight and power consumption, but typically lose out in terms of beam quality. They are suitable for remote or rural field applications of lidar, where the power supply may be unreliable or non-existent and the components may be exposed to the weather conditions.

LDs are similar to LEDs in design and function. Like an LED, a LD utilizes a p-n or p-i-n junction to produce light. They need to be supplied with a high enough current to achieve population inversion, and function like LEDs when supplied with currents below this threshold. The current running through an LD depends on the supplied voltage and the diode temperature. The bandgap is affected by the temperature, and the refractive index of the material is affected by the current. Both of these parameters in turn affect the transmitted wavelength of a LD. The temperature may change during operation, causing wavelength drift. Consequently, the wavelength can be tuned by monitoring the temperature and controlling the supplied voltage. LDs transmit light from the side of the depletions layer, with different divergence along the width and height of the beam as a consequence. The light is typically linearly polarized, which is utilized with multiple polarization bands in Paper II-IV, VI-VII, IX and XI. LDs are available commercially in many wavelengths from the UV to the IR. In this PhD thesis, LDs transmitting at 808 nm were used in entomology in Paper II-IV and VI-XIII. An additional 1550 nm band was employed in Paper II-III and VII. In Paper VI, multiple additional laser bands in the UV and VIS spectral regions were employed in Paper VI, and a 980 nm laser was used in Paper VII.

3.2. Detectors

3.2.1. Photocurrent detectors

Similar to an LED, a photodiode (PD) may consist of a p-n or the better performing p-i-n junction in which an undoped (intrinsic) layer is sandwiched between the p- and n-layers to reduce the response time. A photodiode operates in reverse bias mode, which means that only a small current, I_{PD}, flows through the diode. When light with sufficient photon energy hits the diode it is absorbed, generating electron-hole pairs. This generates a photocurrent, which is

proportional to the intensity of the absorbed light. Sandwich photodiodes (SPD), utilized in Paper II-IV, consist of two semiconductor layers which are sensitive to different wavelength regions, and quadrant photodiodes (QPD), as used in Paper V, consist of an array of 4 PDs arranged in a 2x2 scheme.

A photodiode has a capacitance defined by the cross-sectional area and length of the depletion layer, which relates to its response time. In this PhD work, PDs were implemented with trans-impedance amplifiers (TIA, Figure 3.1) to enhance the obtained signal. A TIA ensures that the voltage over a photodiode, U_{PD}, is constant, which implies that its capacitance is not sensed. Thereby, the bandwidth of the diode is increased (Figure 3.2).

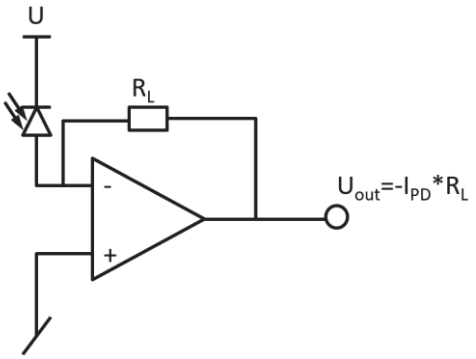

Figure 3.1 Electrical circuit for a photodiode with a trans-impedance amplifier. *A TIA makes use of an operational amplifier to convert the photocurrent produced by a photodiode into an amplified voltage through negative feedback. The output voltage is negative and proportional to the photocurrent, and the amplification is determined by the load resistor.*

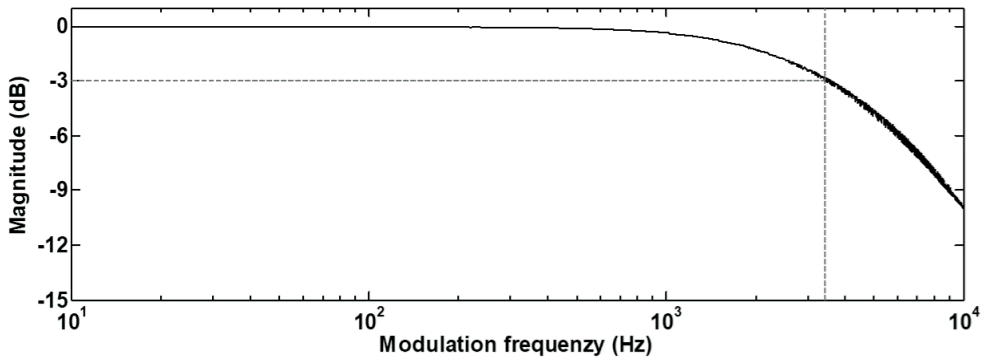

Figure 3.2 Measured bode diagram of a silicon photodiode. *A LED is placed in front of the sensor and modulated at different frequencies, and the magnitude of the photocurrent produced by the PD is measured. The detected magnitude is constant up to ~1 kHz, and thereafter starts to attenuate. The -3 dB line intersects the curve at 3.4 kHz, which defines the bandwidth of the sensor.*

3.2.2. Cascade detectors

Cascade detectors are a class of photonic detectors that rely on incident light generating an avalanche-like process to produce electric signal. In this way, a strong signal can be obtained even from faint light sources. A photomultiplier tube

(PMT) is a device in which the photoelectric effect is utilized to let a photoanode eject electrons when hit by incident light. A negative high voltage (HV) is applied to the photocathode. The ejected electrons are accelerated by an electric field to a series of dynodes, each of which has a successively higher voltage than the previous one. As the original electrons hit the first dynode, their kinetic energy leads to more electrons being emitted and accelerated towards the next dynode. The dynodes are set up such that the number of electrons increases exponentially, until finally arriving at an cathode where the signal is measured. An avalanche photodiode (APD) is a cascade detector based on semiconductor technology. Similar to a regular PD, an APD utilizes a reverse-biased p-i-n junction in which incident light generates electron-hole pairs to produce a photocurrent. However, in an APD a higher, so-called breakdown voltage is utilized. This voltage is strong enough to accelerate the charge carriers to the extent that they knock other bound electrons free, generating more charge carriers in a cascade effect. This leads to a significant growth of the reverse current through the APD. Cascade detectors are sometimes implemented in arrays, such as multi-anode photomultiplier tubes (MA-PMT) and quadrant avalanche photodiodes (QAPD).

3.2.3. Integrating detectors

An integrating detector is a device in which light is absorbed to gradually build up charge over an integration time τ_{int}. After τ_{int}, the built up charge is drained from the sensor, and the amount of charge corresponds to the signal strength. Charge-coupled devices (CCD) and complementary metal-oxide semiconductor sensors (CMOS) are two integrating detector types [117] that have been used in this work. Both types of sensors utilize MOS capacitors, making use of the photoelectric effect to convert incident light into charge. CCD and CMOS detectors are implemented in pixel arrays, either line arrays or 2D arrays, and the main difference between them is the way the accumulated charge is read out from the pixels. On a CMOS chip, each pixel has its own amplification. In contrast, the charge is moved from pixel to pixel on a CCD chip and read out sequentially with the same amplifier. CCDs typically offer higher uniformity between pixels and better noise characteristics, whereas CMOS sensors can be read out faster. The

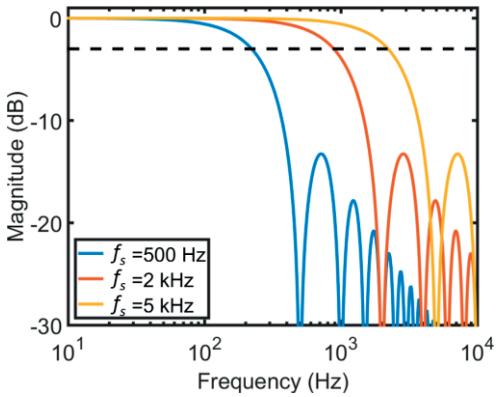

Figure 3.3 Bode plot for an integrating detector, modelled with a sinc function. *According to the model, a 500 Hz sample rate yields a 220 Hz bandwidth, a 2 kHz sample rate yields a 880 Hz bandwidth and a 5 kHz sample rate yields a 2.21 kHz bandwidth. Unlike TIAs, integrating sensors have adjustable bandwidths.*

frequency response of an integrating detector with a rectangular integration profile can be modelled with a sinc function [132], which corresponds to the Fourier transform of a rectangular pulse (i.e. the integration window). Examples with different sample rates are shown in Figure 3.3. Although the side lobes of sinc functions are strongly attenuated, sampling artifacts such as beating and folding of tones may appear when insects exhibiting wing-beat harmonics above the Nyquist frequency are observed with an integrating detector. This is further discussed in Paper XII.

3.3. Systems

3.3.1. Hyperspectral camera

A push-broom hyperspectral camera [133] may be used to investigate the spectral properties of insects *ex-vivo*. A tungsten halogen white-light lamp is used to illuminate a sample. Scattered light was imaged onto a slit, passed through a grating spectrometer and recorded with a 2D sensor array. Two sensors have been used in this PhD work: a Si-CMOS covering the visible and NIR spectral region (400-1000 nm) and a mercury cadmium telluride (MCT) focal-plane array (FPA), covering the SWIR spectral region (900-2500 nm). Thereby, one dimension on the sensor images the sample in one direction, and the other dimension on the sensor

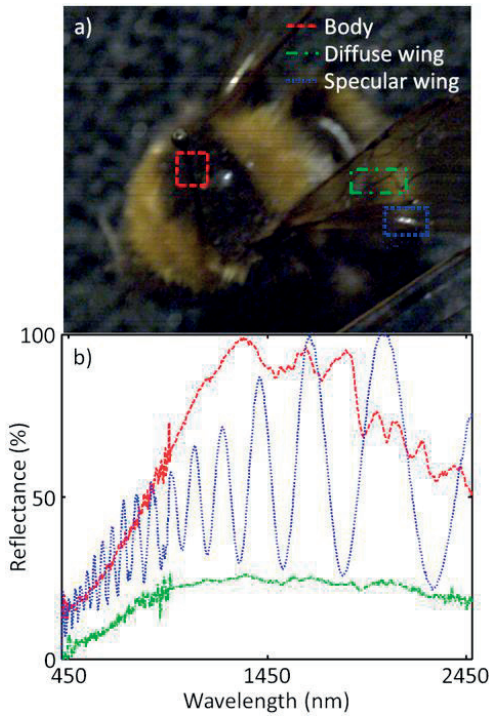

Figure 3.4 Hyperspectral image of a bumblebee with associated spectra. a) *The bumblebee is mounted with a needle on a board and scanned with a push-broom hyperspectral camera. Three regions are marked in the image, which correspond to the spectra shown in b).* ***b)*** *Adjoined spectra of the same sample from two hyperspectral images are displayed: one in the VIS spectral region, and one in the SWIR spectral region. The slope observed in all spectra between 450 nm and 1100 nm is due to melanin absorption. The bumblebee is dried, unlike the sample used for Figure 2.6, which is why no significant water absorption is observed. Spectral fringes are observed from the specular reflex in the wing, as in Figure 2.5. The diffuse reflectance of the wing is comparatively low.*

resolves the sample spectroscopically. The sample is translated in the non-imaged direction, and consecutive images are used to construct hyperspectral images of the entire sample (Figure 3.4).

3.3.2. Entomological *ex-vivo* characterization

The optical properties of insects have been studied *ex-vivo* by many groups [102, 109, 114]. For insect surveillance, heading-dependent reference values are important for classification. To this end, tomographic approaches wherein a sample is mounted and rotated have been employed in the optical- [9] and microwave regimes [134]. In this thesis work, a laboratory *ex-vivo* reference system was built for characterizing the heading-dependent optical cross section (OCS) of insects. The system, which is further described in Paper I, enables acquisition of the scattering phase functions of insects. In addition, the DoLP of different body parts at different scattering angles can be obtained (see thesis cover) and compared to the backscatter OCS of insects at different aspect angles. As such, the system enables the acquisition of excellent reference data which may be used for interpretation of field data. Further improvements to the system may include additional wavelength bands, and another axis of insect rotation. Thereby, tomographic 3D models of insects may be obtained [135].

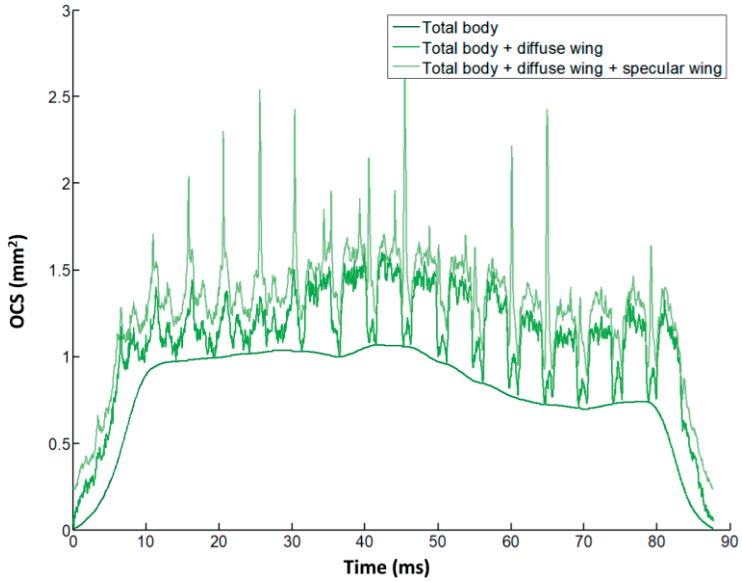

Figure 3.5 Backscatter signal from a fruit fly (Drosophila melanogaster) at 808 nm segmented into contributions from the body, diffuse wing and specular wing. *The polarimetric setup enables the distinction of coherent (specular) and incoherent (diffuse) signal contributions. Whereas the signal from the body is relatively static, the wing signal oscillates with the wing-beat frequency. The incoherent signal from multiple scattered light contributes to both polarization bands, whereas the specular reflections only contribute to the co-polarized band.*

3.3.3. Entomological *in-vivo* characterization

To enable remote identification of insect species of interest, knowledge of their *in-vivo* scattering properties are necessary. Insect wing-beat signals have been recorded in laboratory conditions in transmission- [136-139] and backscatter mode [20]. In this PhD project, a polarimetric and spectroscopic laboratory system was constructed to measure the time-resolved backscatter signal from insects released into the FoV of the system, used in Paper II-IV. The system measures backscattered light in two wavelength- (808 nm and 1550 nm) and two polarization bands (co-polarization and depolarization). Flight tracks are obtained through stereovision [140, 141], which relate to the flight kinematics of insects [142]. The flight heading also relates to the relative phases of wing-beat harmonics, see discussion in Paper V. An additional photodiode is used to measure the extinction, enabling calculation of the reflectance of a target.

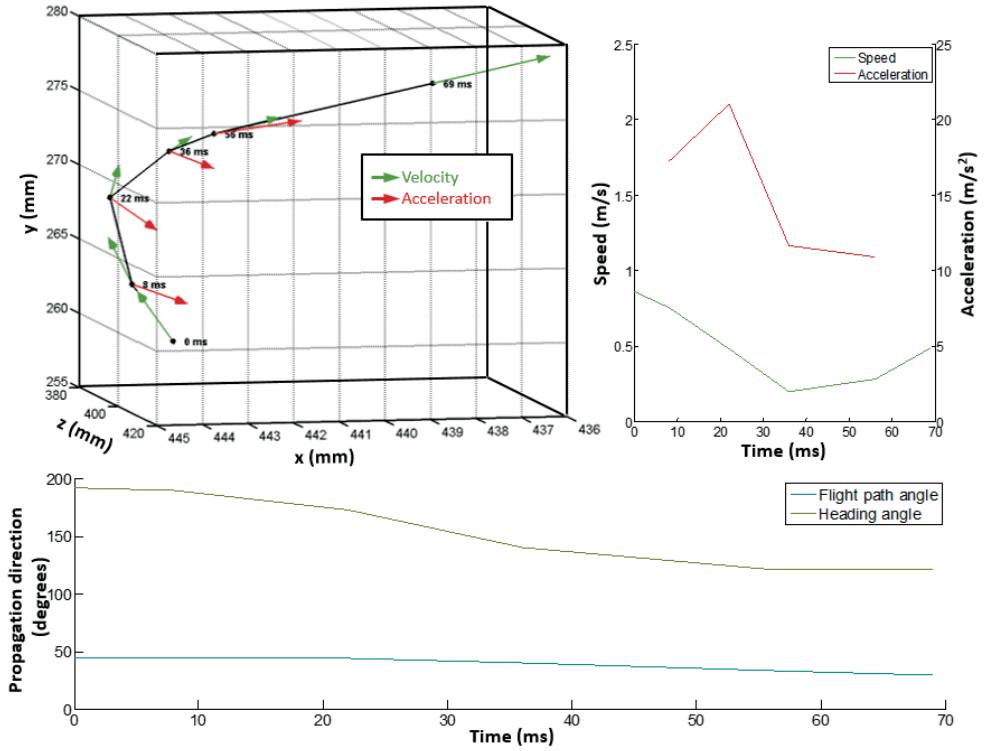

Figure 3.6 3D flight path of a fruit fly (Dr. melanogaster) flying through the laser beam. *Through a folding mirror, a camera monitors insects from above and from the side simultaneously, enabling acquisition of 3D flight paths. The velocity and acceleration is calculated with the time stamp from each measured position. The flight heading of an insect is expected to relate to the frequency contents of the signal, and in particular to the relative phases of the wing-beat frequency and the overtones.*

Insects are released into the probe volume, and the signals are calibrated by dropping diffuse white targets (1/4'' teflon spheres) through the probe volume. The diffuse and specular components of the body- and wing signals of insects are obtained (Figure 3.5). Thereby, signal parameters such as the WBF and OCS of insect bodies and wings in all bands can be derived. Figure 3.6 shows the flight track of an insect, from which the heading angle, flight path angle, velocity and acceleration is acquired.

3.3.4. Passive lidar

Passive detection is employed in the microwave [30], acoustic [36] and optical regime [128-130, 143, 144]. In passive radar [145, 146], the phase difference between the signals detected in two or more radar array elements is used to extrapolate the location of a scattering object. A similar concept is used in bioacoustics to localize birds from their calls [38]. In this PhD project, passive ranging was accomplished in the optical regime with a quadrant photo diode (QPD) under a clear sky with a FoV uniformly illuminated by the Sun (Paper V). The technique is time-resolved, *in-vivo* and *in-situ*. In principle, passive lidar can be achieved with any combination of telescope and quadrant sensor. However, ranging is most consistent when the termination is placed at the limit between the near- and far field. Reliable flight speed estimates may be obtained when both the sensor and aperture are quadratic, ensuring that the FoV is quadratic along the entire range. If aimed upwards into the sky, i.e. not using a termination cavity, active light sources like LEDs and lasers may be implemented to enable night-time usage. Overall, the method is a simple and robust "poor-man's entomological lidar" which can be adapted to many applications and measurement geometries.

3.3.5. Scheimpflug lidar

Scheimpflug lidar (Figure 3.7) is a technique that was developed in the past ten years [12, 147]. In this technique, a continuous wave (CW) laser beam is transmitted across a field, and a line sensor monitors an air volume illuminated by the laser. Range resolution is achieved by Scheimpflug criterion and Hinge rule [148, 149]. Thereby, infinite focal depth is achieved, with each pixel on the sensor monitoring a specific section of the laser beam.

In conventional lidar, pulsed lasers are used [150]. The time between transmission of a laser pulse and detection of an echo signal is used to calculate the distance through the known speed of light. Using nanosecond-scale pulses yields a range resolution of about 1 m. The temporal resolution of pulsed lidar is limited by the pulse repetition rate and the roundtrip time of the pulse. In Scheimpflug lidar the pixel foot prints grow with distance from the system. At close range (~0-200 m) the range resolution is in the order of a few centimeters, whereas further away the

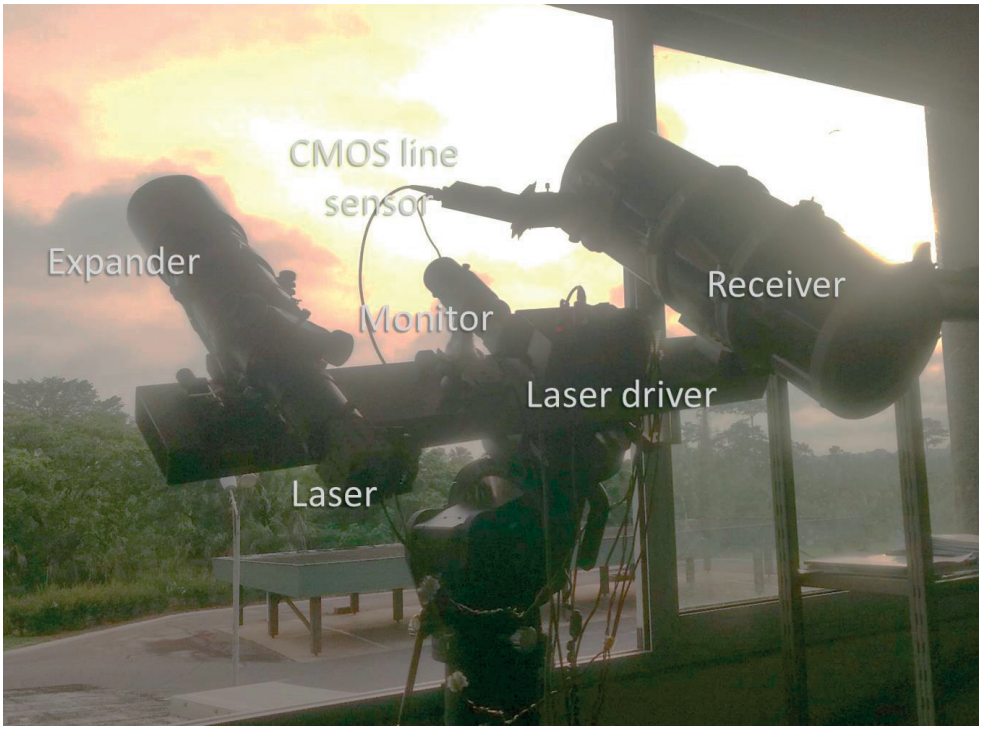

Figure 3.7 Scheimpflug lidar system in the evening sun in Ivory Coast. *Light from a laser diode is expanded and collimated with a refracting telescope. Backscattered light is collected by a Newtonian receiver telescope and imaged onto a CMOS line sensor. The laser output is controlled with a laser driver, able to operate in CW mode or with two or more time slots. The laser is switched on and off intermittently so that the optical background is recorded every second exposure, which corresponds to operation with two time slots. When operating with three or more time slots, the extra slots correspond to additional spectral- or polarization bands.*

range resolution is in the order of meters or tens of meters. The temporal resolution is limited by the sample rate of the detector. In a recent study, a side-by-side comparison of pulsed lidar and Scheimpflug lidar was performed [151]. The study found the methods comparable in most regards, indicating that the main advantage of Scheimpflug lidar is the lower cost and complexity.

Scheimpflug lidar is a versatile tool that has been used for *in-vivo* and *in-situ* studies of insects, in aquatic environments [15] and for combustion diagnostics [152]. Differential absorption lidar (DIAL) to measure atmospheric CO_2 concentrations was accomplished in a Scheimpflug configuration using a tunable laser diode [153]. Light-weight and compact implementations have been mounted on drones to scan vegetation from above [154].

Entomological Scheimpflug lidar has been implemented with dual polarization bands [155], as used in the work reported in Papers IX and XI, and with dual

spectral bands [156], as used in the studies described in Paper VII. The laser is modulated on and off to enable background subtraction. High sample rates are used in most entomological applications in order to resolve insect wing beats (Figure 3.8).

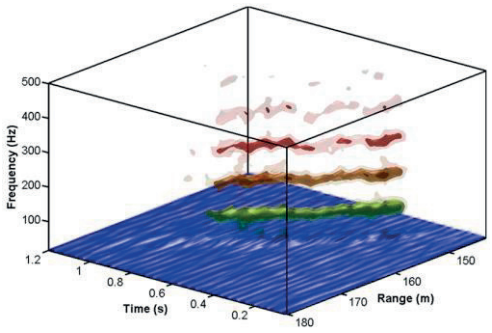

Figure 3.8 Lidar signals from an insect flying through the laser beam. *Insect signals are sparse in space and time, and modulated with the insect wing beat frequency, giving rise to signal bursts with different frequency contents than the optical background. In this case, the wing-beat frequency is about 100 Hz, and several overtones are observed*

4. Data processing

4.1. Data types

The data produced by several methods described in Chapter 3 share many similarities. They are time-resolved at kHz rates and incorporate multiple channels – either different spectral- or polarization bands, or sensor elements observing different spatial locations (Figure 4.1). Depending on the sample rate and the number of channels, the data are stored in files spanning between a few seconds and a few minutes. The majority of the data is empty, and insects flying through the FoV give rise to sparse signal snippets with higher intensity [157]. The data needs to be reduced for efficient processing, and the observed insects extracted and stored separately from the raw data.

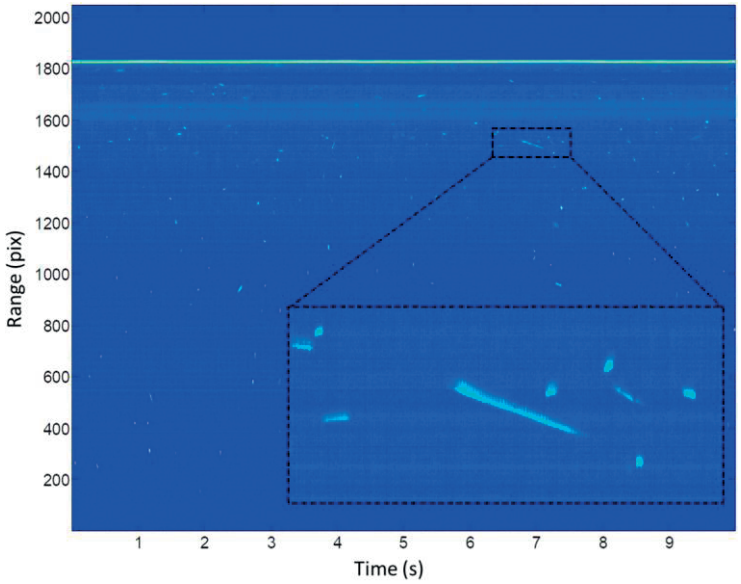

Figure 4.1 Entomological lidar data file from Tanzania. *With a sample rate of 3.5 kHz, 16bit data was acquired using a CMOS sensor with 2048 pixels. The data file contains 35000 time exposures, corresponding to 10 seconds of measurement. Insects appear in the data as brief regions of high intensity. This particular data file was recorded during very high insect activity at dusk. The color scale has been adjusted to enhance contrast.*

4.2. Observation extraction

Different methods of extraction of sparse features in entomological optical remote sensing data have been implemented since the first experiments [129, 157, 158], and have been gradually refined (Paper VIII) to where they are today (Paper IX-XIII). To find and extract insect observations in time-resolved data, the fact that most of the data is empty is utilized. In each data file, a detection threshold is

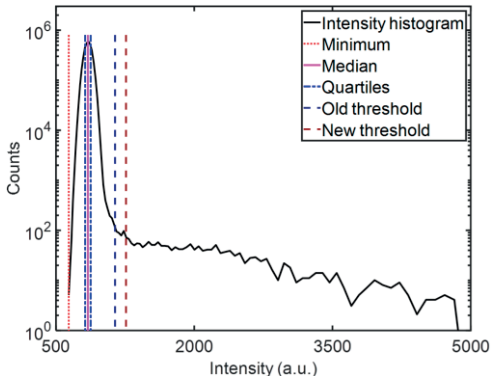

Figure 4.2 Intensity distribution of lidar data, illustrating the two thresholding methods. *The noise level is represented by the distribution around the median, and a detection threshold is defined according to Equation (4.1), from the measured intensities shown in Figure 4.1. The signal exceeding the threshold is interpreted as an insect flying through the laser beam, and evaluated further.*

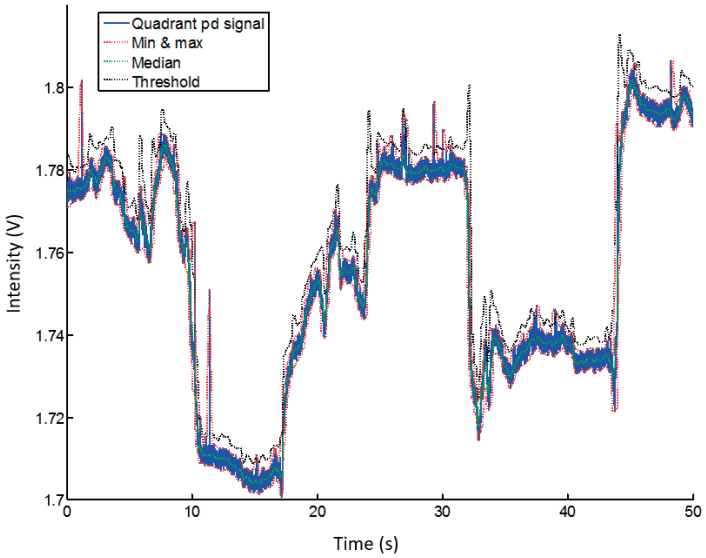

Figure 4.3 Signal fluctuations in passive lidar. *Because the sunlight travels through the entire atmosphere before impinging on the FoV at ground level, the optical background signal is affected by the passage of clouds, heat convection, and other atmospheric phenomena, and therefore undergoes fluctuations. A static detection threshold is unable to distinguish insects from background in these conditions, so a dynamic threshold using sliding statistics has to be used.*

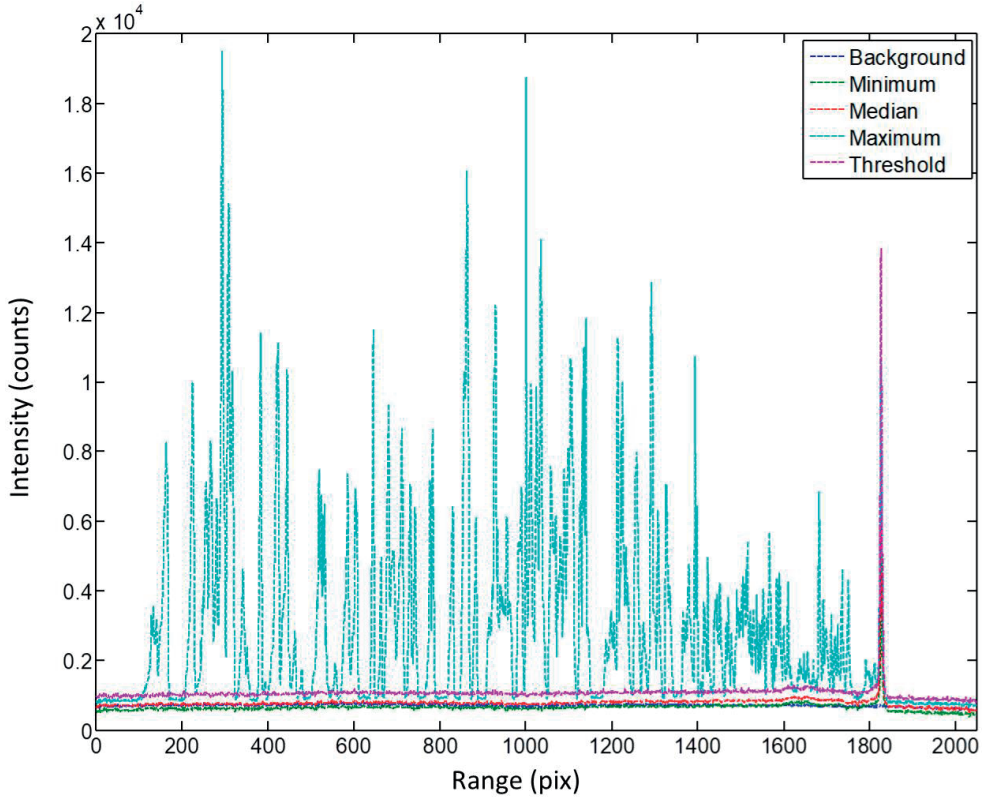

Figure 4.4 Statistical curves from the data file shown in Figure 4.1. *Statistical curves for the entomological Scheimpflug lidar data file illustrated in Figure 4.1. The detection threshold is set with the IQR method, according to Equation (4.1), and all instances where the signal exceeds the threshold are shown in the maximum curve.*

defined based on statistics from the measured light intensities in the file. The expectation value of the empty data is represented by the median signal, I_{med}, in each pixel or band, and is unaffected by outliers i.e. high intensities obtained from insects flying through the FoV. In the early stages of this PhD project (Paper V and VIII), the noise amplitude I_{noise} was approximated as the difference between the median and minimum intensity, I_{med}-I_{min}. Later on in the project (Paper XIII), I_{noise} was represented by the inter-quartile range (IQR), I_{iqr}, of the signal (Figure 4.2). The reason for the change is that I_{iqr} is robust against negative signal spikes and signal fluctuations arising from e.g. smoke from cooking fires drifting into the FoV, or clouds partially blocking the sun in passive measurements. In case of rapid signal fluctuations, such as those commonly obtained in passive lidar measurements (Paper V), a sliding median may have to be employed instead of the overall median intensity (Figure 4.3). In that case, the window size must be selected with care and adjusted to the signal fluctuations. The detection threshold is defined according to Equation (4.1), where K represents the desired SNR.

$$I_{thresh} = I_{med} + K * I_{noise} \quad \textbf{(4.1)}$$

All signal segments exceeding the detection threshold are extracted from the data for further analysis. In lidar measurements the statistical curves (Figure 4.4) are recorded and used to overview the entire dataset (Figure 4.5). The process of going from raw lidar data to parameterized insect observations is illustrated fully in Figure 4.6.

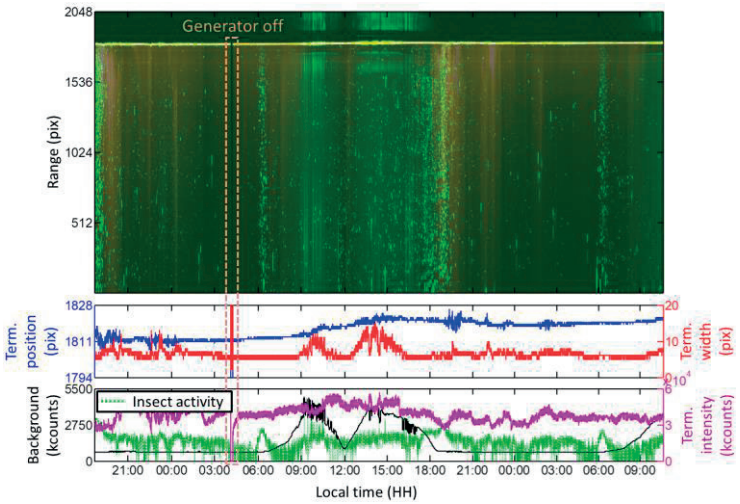

Figure 4.5 Statistical overview of approximately 42 hours of lidar data, wherein each data column represents one 10-second data file. Top*) False-color image of the statistical median, maximum and minimum vectors from all data files shown in red, green and blue, respectively. Green dots correspond to insects flying through the laser beam, and the line just beyond pixel 1800 corresponds to the echo from the termination target. Increased insect activity is observed at dawn and dusk. The generator powering the system ran out of gas at one point in the middle of the night and had to be refuelled.* ***Middle****) Stability plots for the lidar system, showing the pixel position and width of the termination echo. The position of the termination echo on the sensor is stable, drifting about 10 pixels over 42 hours. The termination echo width during the day is about twice as large as during the night.* ***Bottom****) The termination intensity and insect activity is shown in relation to the background light level. The background light level decreases at noon due to a solar eclipse. Clear crepuscular activity peaks among the insects are observed.*

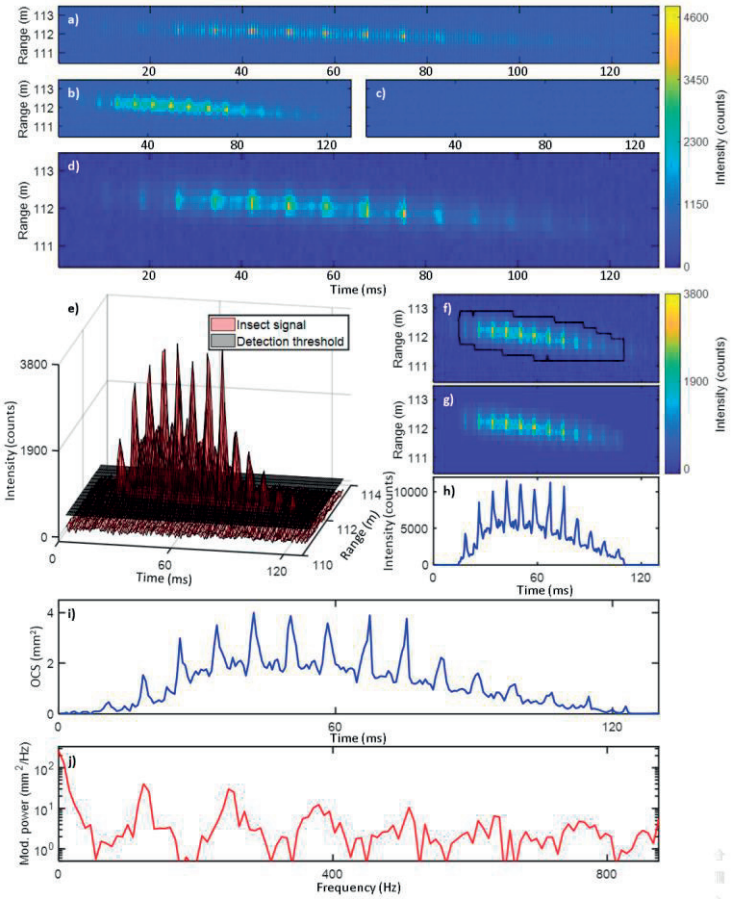

Figure 4.6 Illustration of the entire observation extraction procedure in entomological lidar. ***a)*** *Raw data, in which every second exposure corresponds to when the laser is on and off, respectively.* ***b-c)*** *The raw data is sorted into the on- (**b**) and off components (**c**).* ***d)*** *The optical background is acquired from (**c**) through interpolation, and subtracted from (**b**).* ***e)*** *A detection threshold with an SNR=2 is generated. A detection mask is generated to map all data segments which exceed the threshold.* ***f)*** *The detection mask (black line) indicates all instances of the signal exceeding the threshold. Image erosion and dilation are used to adjust the detection mask, filtering out signal segments too short to be of interest.* ***g)*** *The detection mask is used to crop out signal regions of interest.* ***h)*** *The signal is summed along the range axis, generating a time series.* ***i)*** *The signal intensity is calibrated into an optical cross section.* ***j)*** *Power spectrum of the time series in (**i**), with peaks at the insect wing-beat frequency and its overtones.*

4.3. Range calibration

4.3.1. Passive lidar

Range information is needed to quantify the scattering cross section of a target. Acquiring the range passively in optics is challenging. Early approaches include coincidence rangefinders [159], whereas some approaches like nephelometry and cytometry [160] limit the probe volume to a point, and other methods such as digital in-line holography utilize post focussing [161]. In Paper V of this thesis, passive lidar was accomplished with quadrant. The method is enabled by three assumptions:

1. Insects are small enough to be considered as point sources when flying through the probe volume.

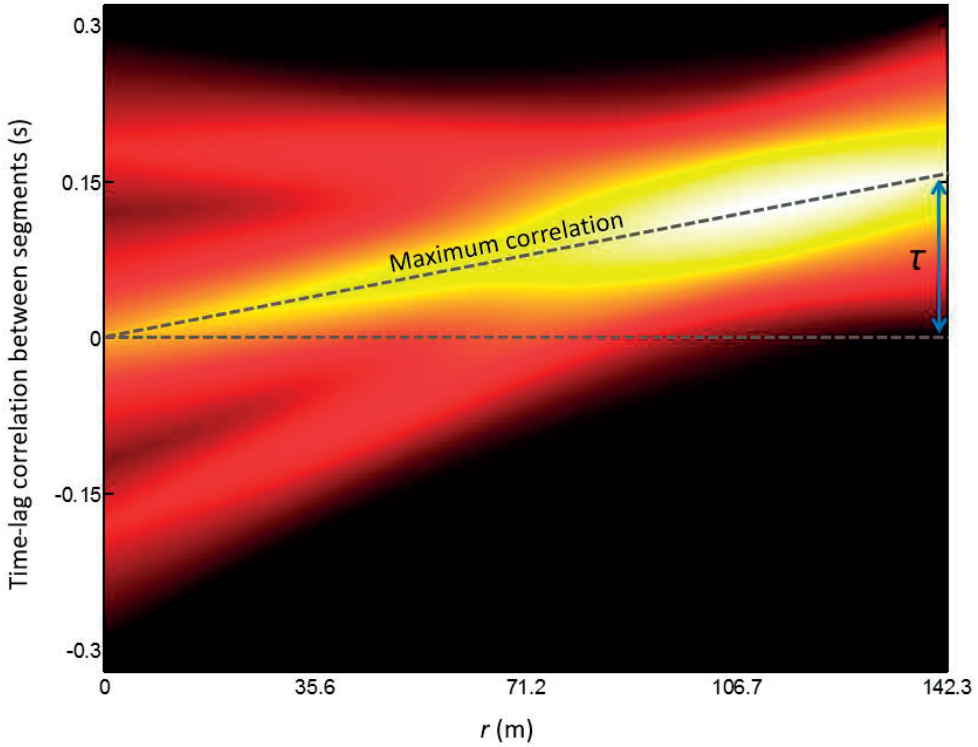

Figure 4.7 Time-lag correlation of detector segments. *The signals from two adjacent detector segments are compared. One of the signals is kept fixed, and the other is gradually scanned by increasing the time delay. The correlation is calculated at each point, and the maximum correlation corresponds to the time delay with which the two signals are the most similar. In this figure, the simulated FoVs of two adjacent detector elements are time-lag correlated, illustrating that the time delay τ corresponding to the maximum correlation increases linearly with the distance from the sensor.*

2. Insects fly straight through the probe volume with a constant velocity vector.
3. The coaxial movement of insects is insignificant compared to the length of the probe volume.

The FoV of two adjacent detector elements can be simulated. The sensor is fully out of focus at the telescope aperture, and focused at the entrance of a dark termination cavity. Therefore, the FoV of the two detector elements are identical and overlap fully at the aperture, and identical but sharply separated at the termination. As such, an insect flying through the FoV at the aperture will appear simultaneously in both detector elements, whereas at the termination it will appear in one element after the other. The quotient between the time delay between

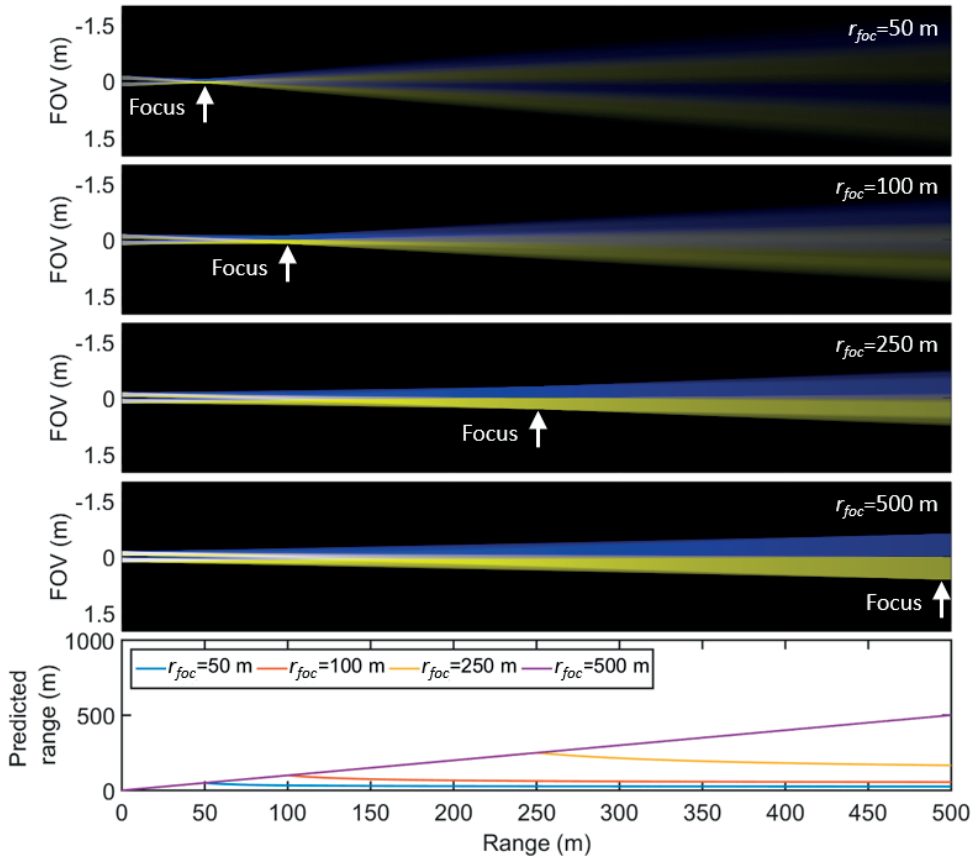

Figure 4.8 The effect of the focal distance on the range prediction. *The FoV of two adjacent sensor elements is simulated with raytracing. Four cases are presented in which the sensor is focussed at different distances. The bottom panel shows the predicted range compared to the actual range in the simulation, demonstrating that the passive ranging equation is invalid beyond the focal distance of the sensor.*

adjacent detector segments τ (Figure 4.7) and the transit time Δt of an insect observation is a unique fingerprint for each distance since the flight speed of the insect cancels out. The passive lidar equation, Equation (4.2), estimates the distance $\hat{r}$ to an insect with the signal parameters τ and Δt, the telescope focal length f and aperture $\emptyset_{tel}$, the sensor diameter d_s and the focal distance r_{foc}. At distances beyond r_{foc}, the FoV of the two segments again start overlapping, and the ranging becomes ambiguous as the quotient $\tau/\Delta t$ goes toward an asymptotic value (Figure 4.8).

$$\hat{r} = \frac{\tau \emptyset_{tel} f}{\tau \left(\frac{\emptyset_{tel} f}{r_{foc}} - d_s \right) + \Delta t \frac{d_s}{2}} \tag{4.2}$$

Paper V illustrates that the ranging accuracy has advantageous properties when the sensor is focused at the distance between the near field and far field, i.e. $r_{foc}=r_{lim}$. The distance r_{lim} is calculated according to Equation (4.3). Since the ranging becomes ambiguous beyond r_{foc}, and $r_{foc}=r_{lim}$ yields consistent ranging accuracy, the best results are obtained when the sensor and telescope are selected so that r_{lim} matches the desired measurement geometry. If a long FoV is desired, a small sensor and a telescope with a large aperture and a long focal length are beneficial.

$$r_{lim} = \frac{f(\emptyset_{tel} + d_s)}{d_s} \tag{4.3}$$

4.3.2. Scheimpflug lidar

In Scheimpflug lidar, each pixel on the sensor monitors a different air volume, sharply imaging a different section of the laser beam. This is made possible through arrangement of the system according to the Scheimpflug principle and the Hinge rule [147, 149, 162]. In short, the Scheimpflug principle states that the lens plane defined by the receiver telescope, the image plane defined by the tilt of the detector, and the object plane defined by the laser beam must intersect. Further, the Hinge rule adds the requirement that the front focal plane, which is parallel to the lens plane and intersecting the focal point of the receiver telescope, must intersect the object (laser) plane and the plane parallel to the image plane that intersects the center of the lens plane. This is illustrated in Figure 4.9.

The relative position and alignment of the lidar components have implications for the distance to the air volumes observed by the pixels. The angle θ_{lens} between the lens plane and the laser beam is given by Equation (4.4), calculated from the detector tilt angle φ_{det}, the distance between the center of the receiver lens and the center of the sensor d and the focal length of the receiver telescope f_{rec}. The baseline h, i.e. the distance between the center of the lens and the laser beam is calculated according to Equation (4.5). With the distance ρ_{pix} of each pixel from

the center of the sensor, the distance r_{pix} is calculated according to Equation (4.6) [147, 149].

$$\theta_{lens} = \tan^{-1}\left(\frac{f_{rec}\tan(\varphi_{det})}{d - f_{rec}}\right) \tag{4.4}$$

$$h = \sin(\theta_{lens})\frac{d}{\tan(\varphi_{det})} \tag{4.5}$$

$$r_{pix} = h\frac{d + \rho_{pix}(\sin(\varphi_{det}) - \cos(\varphi_{det})\cot(\theta_{lens}))}{d\cot(\theta_{lens}) + \rho_{pix}(\cos(\varphi_{det}) + \sin(\varphi_{det})\cot(\theta_{lens}))} \tag{4.6}$$

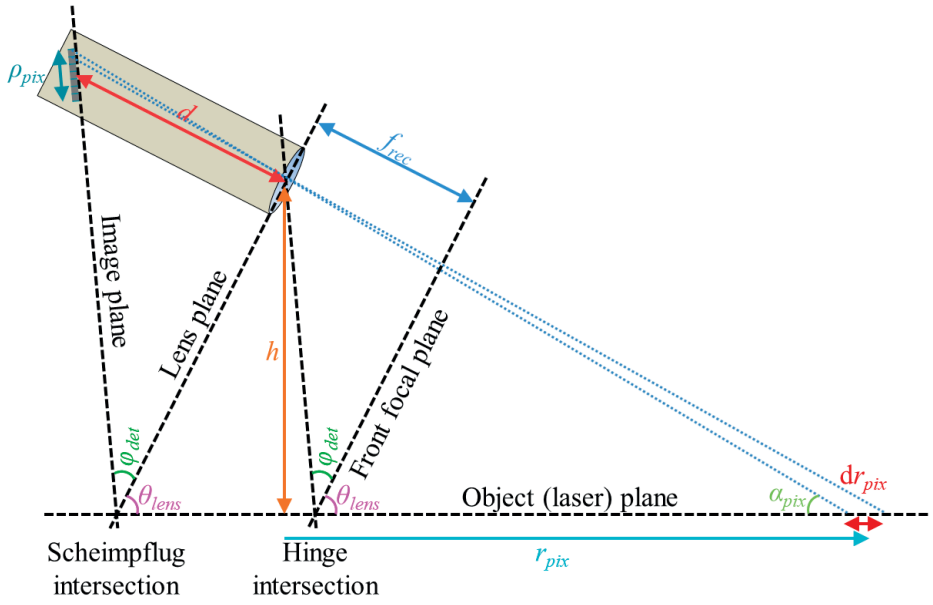

Figure 4.9 Schematic illustration of how the Scheimpflug principle and Hinge rule are implemented in Scheimpflug lidar. *When the planes align in the Scheimpflug- and Hinge intersection, infinite focal depth along the laser beam is achieved. Thus, each pixel on the sensor monitors a specific section of the laser beam with sharp focus.*

Further, the range resolution of the system, dr_{pix}, is acquired by taking the derivative of r_{pix} with respect to ρ_{pix}, see Equation (4.7). In this equation, $d\rho_{pix}$ equates to the pixel pitch p on the sensor. Whereas Equation (4.7) is the ideal range resolution, the effective range resolution is limited by the laser beam width. Each pixel on the sensor monitors the laser beam at an angle α_{pix}. With a beam width of $w(r)$, the effective range resolution dr_{eff} is given by Equation (4.8).

$$\mathrm{d}r_{pix} = \frac{r_{pix}^2 d\cos(\varphi_{det})\left(1+\cot^2(\theta_{lens})\right)}{h^2\left(d+\rho_{pix}(\sin(\varphi_{det})-\cos(\varphi_{det})\cot(\theta_{lens}))\right)^2}\mathrm{d}\rho_{pix} \quad \textbf{(4.7)}$$

$$\mathrm{d}r_{eff} \approx \frac{w(r)}{\alpha_{pix}} \quad \textbf{(4.8)}$$

4.4. Size calibration

4.4.1. Angular size

One size estimate in Scheimpflug lidar data that can be calculated without an intensity reference is called the angular size δ (AS), which relates to a similar measure used in astronomy [163]. The smallest observable AS is the foot print of one pixel at each distance, calculated from the magnification of the receiver telescope in a Scheimpflug setup, the pixel pitch of the sensor ρ, and adjusted for the tilt angle of the sensor φ. The upper limit corresponds to the width of the laser beam at each distance (Figure 4.10). The AS of an insect observation δ_{obs} corresponds to the maximum number of pixels (n_{pix}) it is observed by simultaneously during its transit through the laser beam, see Equation (4.9).

$$\delta_{obs} = Mpn_{pix}\cos(\varphi_{det}) \quad \textbf{(4.9)}$$

where M is the magnification of the telescope at the distance of the observed insect. The angular size is a useful size estimate in Scheimpflug lidar because it can be calculated without the need for an intensity reference. It is, however, affected by poor focus. Subpixel precision can be achieved by calculating the statistical moment.

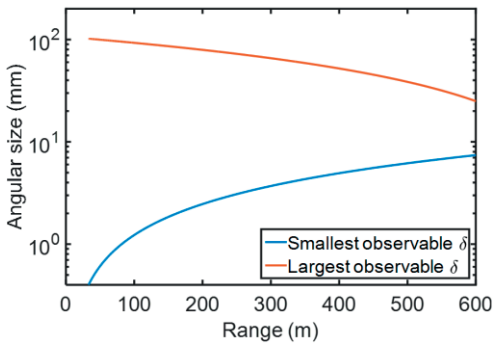

Figure 4.10 The minimum and maximum angular size δ along the FoV. *The angular size δ of an observed insect corresponds to the size of the number of pixels the insect is observed by, projected to the distance at which it is observed. The lower limit corresponds to the footprint of a single pixel, whereas the upper limit corresponds to the laser beam width at each distance.*

4.4.2. Optical cross section

The optical cross section σ is a quantitative size estimate, analogous to the radar cross section [21, 134] obtained with entomological radars. The OCS is the

product of the illuminated area of an insect and the probability of scattering light into the sensor [164]. In backscatter geometries, the scattering probability is equivalent to the reflectance of an insect. The OCS is obtained by comparing the scattered light intensity from the insect to the intensity obtained from a target with known size and reflectance. The scattering probability, or reflectance, depends on the wavelength, and the illuminated area depends on the orientation of the insect and the phase in the wing-beat cycle. The scattering probability also depends on the illumination angle, as demonstrated in Paper I. For instance, small organisms like mosquitoes exhibit much larger OCSs in forward scatter geometries, since the light is less likely to interact with the tissue in smaller volumes. For these organisms, most of the light is ballistic and passes straight through without interacting with the organism. For intermediate sized insects, the light undergoes multiple scattering before exiting the insect. The largest insects are opaque, and backscattering becomes the dominant part as the size increases.

In this PhD project, white paper with 97% diffuse reflectance and teflon spheres with an assumed 100% Lambertian reflectance have been used for calibration in the laboratory work. In lidar field applications, black neoprene termination targets with 1.8% diffuse reflectance at 808 nm have been used. Since insects in the laboratory are observed at approximately the same distance from the sensor as a reference target, σ_{obs} can be calculated according to Equation (4.10).

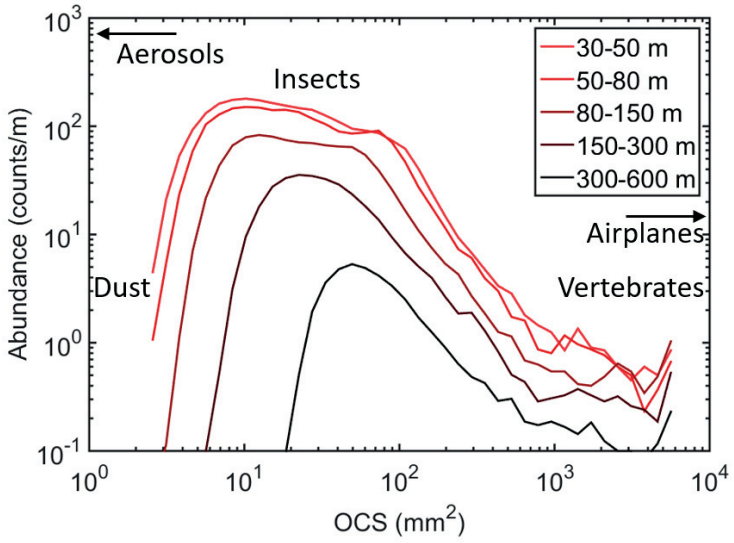

Figure 4.11 OCS histograms at different distances from a lidar system. *In lidar, the sensitivity has a r^{-2} dependence and decreases significantly with distance from the system. The smallest organisms may therefore only be observable close to the system. As seen in this figure, insects down to a few mm^2 are detected at close range, whereas only larger insects are detected far away. Assuming homogeneous biomass spectra at different ranges, the decrease in counts/m can be attributed to the system sensitivity.*

$$\sigma_{obs} = \frac{I_{obs}}{I_{ref}} \sigma_{ref} \quad \textbf{(4.10)}$$

where I_{obs} and I_{ref} are the measured light intensities from the insect and reference target, respectively, and σ_{obs} is the OCS of the reference target.

In entomological lidar measurements, the distance to an observed insect must be taken into account. If the insect is located at a distance r_{obs} from the lidar system, the reference target is located at a distance r_{ref} from the lidar system and the static air signal at the distance of the observed insect is given by I_{st}, the OCS is calculated according to Equation (4.11) under the assumption of a homogeneous atmosphere [165].

$$\sigma_{obs} = \frac{I_{obs}}{I_{st}} \frac{r_{obs}^2}{r_{ref}^2} \sigma_{ref} \quad \textbf{(4.11)}$$

Figure 4.12 Neoprene-covered lidar terminations board mounted in a tree in Ivory Coast. *Neoprene is a diffuse scattering target with low reflectance, making it ideal as a termination target in entomological lidar to prevent signal saturation.* ***a)*** *The author is climbing a homebuilt bamboo ladder to mount the neoprene-covered board several meters above ground. Doing so ensures eye safety during measurements.* ***b)*** *The laser beam is centred on the termination target during lidar measurements. The dimensions of the laser spot are used in conjunction with neoprene reflectance to calibrate optical cross sections of insects.*

Like the angular size, the minimum observable OCS increases with distance due to read-out noise and decreasing instrument sensitivity (Figure 4.11). Since the OCS is calibrated with a diffuse reference target, the diffuse components of insect signals are best suited for comparison. These can readily be isolated from the specular components in polarimetric measurements, and through frequency analysis in non-polarimetric measurements. Using the neoprene termination target (Figure 4.12) as intensity reference is not always ideal – for instance, when the neoprene is wet from rain or dew it has been observed to have significantly higher reflectance. However, dropping other calibration targets through the beam may be challenging [143]. In vertical lidar measurements (Paper X) it is very impractical due to the typical near limit of 30-50 m. In horizontal measurements the beam is more accessible, but still propagates at least 3-5 m over ground for eye safety purposes.

4.5. Frequency analysis

The wing-beat frequencies of insects with associated higher harmonics are crucial classification parameters [137, 166]. When the WBF of an insect is known, a parameterization model can be applied to the signal based on the obtained frequency. This enables the signal to be condensed into a discreet set of parameters corresponding to the strengths and phases of the WBF and its higher harmonics. However, obtaining reliable WBFs is far from a simple task [167, 168]. The fundamental tone is not always the strongest one (Paper V) [164], and varies with ambient temperature and insect weight [169, 170]. In this PhD project several approaches to fundamental wing-tone estimation have been pursued (Paper VIII, Paper XII-XIII).

4.5.1. Parameterization model

In this PhD work, insect signals have been modelled with a parameterization model, condensing the raw signals into a discrete set of components (Paper VIII) [164]. A fundamental frequency f_0 is defined as per Chapter 4.5.2-4.5.4. The signal σ_{obs} is filtered with a sliding minimum and a sliding maximum filter, with window size $w=f_s/f_0$, in which f_s is the sample rate used in the measurement. The envelope of the signal is calculated as the convolution of a normal distribution with full-width half maximum (FWHM) equal to w, and the average of the sliding minimum filtered and sliding maximum filtered signals. A regressor ψ of basis functions is defined, containing a Fourier series of f_0 and its overtones up to the Nyquist frequency f_{Ny}. Regression is further detailed in Chapter 4.6.3. The envelope is normalized, and all basis functions are weighted with the normalized envelope according to Equation (4.12), in which $b=[b_1,b_2,\ldots,b_l]$ is the envelope and $t=[t_1,t_2,\ldots,t_l]$ is the time. The index n denotes the harmonic number, and m indicates the odd (sine) and even (cosine) harmonic components.

$$\psi_{l,n,m} = \begin{bmatrix} b_1 & b_1\sin(2\pi f_0 t_1) & b_1\cos(2\pi f_0 t_1) & b_1\sin(2\pi 2 f_0 t_1) & \cdots & b_1\cos(2\pi n f_0 t_1) \\ b_2 & b_2\sin(2\pi f_0 t_2) & b_2\cos(2\pi f_0 t_2) & b_2\sin(2\pi 2 f_0 t_2) & \cdots & b_2\cos(2\pi n f_0 t_2) \\ \vdots & \vdots & \vdots & \vdots & \ddots & \vdots \\ b_l & b_l\sin(2\pi f_0 t_l) & b_l\cos(2\pi f_0 t_l) & b_l\sin(2\pi 2 f_0 t_l) & \cdots & b_l\cos(2\pi n f_0 t_l) \end{bmatrix} \quad \textbf{(4.12)}$$

A coefficient a_n for each basis function is obtained through QR factorization by projecting the insect signal onto the basis function, as shown in Equation (4.13). The sine and cosine pair of coefficients for each harmonic of f_0 can then be used to calculate the strength and phase of each harmonic in the insect signal. A reconstructed time series $\hat{\sigma}$ is obtained according to Equation (4.14) (Figure 4.13).

$$a_{n,m} = (\psi_{n,m}^T \psi_{n,m})^{-1} \psi_{n,m}^T \sigma_{obs} \quad \textbf{(4.13)}$$

$$\hat{\sigma} = \sum_{n,m} a_{n,m} \psi_{n,m} \quad \textbf{(4.14)}$$

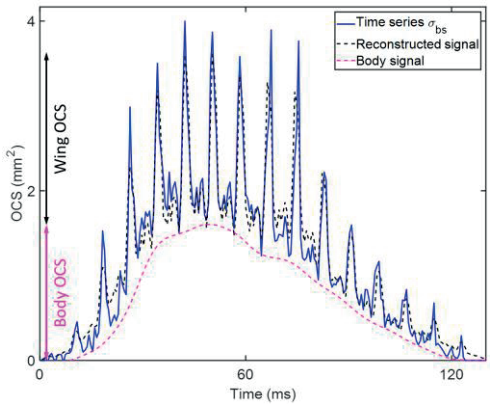

Figure 4.13 Original and reconstructed insect signal. *The original time series is acquired from the data and calibrated. The wing-beat frequency f_0 is obtained, after which the signal is reconstructed with a Fourier series containing the signal envelope and the sine- and cosine components of f_0 and its overtones up to the Nyquist frequency. The body signal is obtained by applying a sliding minimum filter to the signal with a window size equal to the period of f_0. The body- and wing OCS can then be acquired as the maximum of the body- and wing components, respectively, of the signal.*

4.5.2. Power thresholding

In the frequency estimated described in Paper VIII, the power spectrum of an insect signal was obtained with a fast Fourier transform (FFT). A threshold, similar to the one used in the observation extraction procedure, was set in the power spectrum. This threshold was used to find the modulation peaks corresponding to f_0 and its overtones. An initial estimation of the WBF, f_{0init}, was obtained as the median distance between the peaks. The parameterization model was applied with a range of test frequencies f_{test} between f_{0init}±30%. f_0 was then set as the test frequency yielding the smallest residual when compared to the original signal.

4.5.3. Analysis of residuals

Residual analysis was developed in [168], and further refined in Paper XIII. In this method, the parameterization model is implemented with a set of test frequencies, f_{test}, calculating the residual for each test frequency. The model contains inherent biases toward both low and high frequencies – at low test frequencies, the regressor contains many degrees of freedom, and at high frequencies the window size is small, resulting in an envelope that in itself matches the signal well. The regressor error is modelled analytically, and the window error is obtained using the signal envelope. These two errors are used to adjust the residual vector, and f_0 is obtained as the test frequency with the smallest adjusted residual (Figure 4.14).

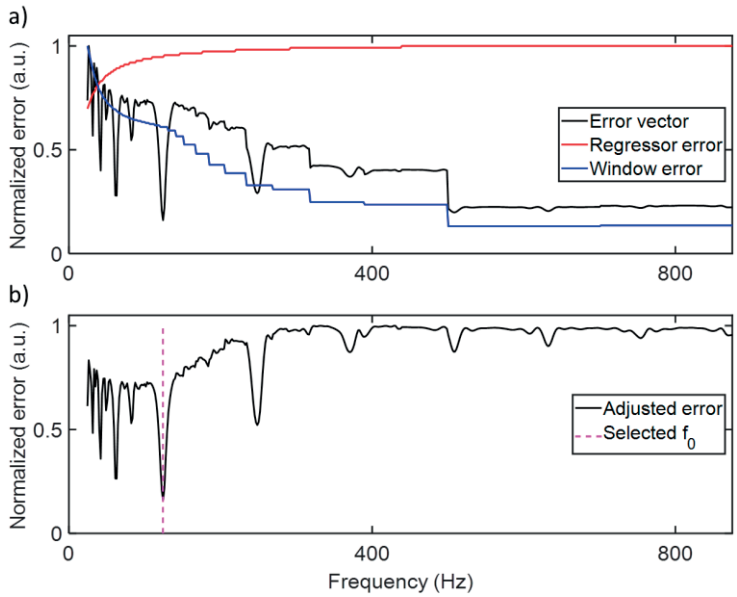

Figure 4.14 Residual vectors and model biases. a) *Initial error vector, regressor error and window error as function of test frequency. The regressor error indicates that there is a bias toward lower frequencies, and the window error indicates that there is a bias toward higher frequencies.* ***b)*** *The adjusted error vector. By eliminating the biases inherent to the model, the wing-beat frequency f0 can be selected with much improved accuracy.*

4.5.4. Modulation spectrum with fixed frequency vector

Due to the difficulty in obtaining reliable fundamental frequency estimates, an alternative approach circumventing the issue was developed in Paper XII-XIII. A frequency vector was defined between the lowest observable frequency defined by the transit time and the Nyquist frequency defined by the sample rate. The number of bins corresponded to the typical length of an insect signal in a given data set.

For each insect signal present in the collected data, a corresponding noise vector was obtained just before or after the insect flew through the beam, at the same distance. Welch's method [171] was used to estimate the power spectral density at the frequencies in the frequency vector for both the insect and noise signals. Each insect power spectrum was normalized with a linear fit of the corresponding noise power spectrum, yielding power spectra that could then be used for classification.

4.6. Factorization and classification methods

In data sets with many observations and many observed parameters, factorization methods are useful for reducing the data to facilitate interpretation, and classification methods are used to group observations together based on statistical similarity.

4.6.1. Data factorization

Principal component analysis (PCA) and singular value decomposition (SVD) are fundamental tools in multivariate analysis [172, 173], and reduce a data set to a lower number of variables containing most of the information. In a data matrix X, wherein each row corresponds to an observed insect and each column corresponds to the modulation power at a given frequency, the SVD approach calculates three matrices U, S and V according to Equation (4.15).

$$X = USV^{\mathrm{T}} \tag{4.15}$$

The columns of V are the modulation spectra that best describe the entire data set, in decreasing order of importance. The diagonal matrix S contains the eigenvalues of the data set, the magnitude of which equates the overall importance of each modulation spectrum in V. The rows in U relate to the observed insects, where the value in each column indicates how much of the corresponding modulation spectrum in V is found in the modulation spectrum of each insect. By only including modulation spectra with high eigenvalues, data sets with large numbers of variable may be reduced to only a few (Figure 4.15).

4.6.2. Unsupervised classification methods

Hierarchical cluster analysis (HCA) is an unsupervised clustering method in which the observed variables are treated as dimensions in a multidimensional space [129, 174]. Each observation then corresponds to a coordinate in this multidimensional space. The statistical distance between one observation and all others is calculated with a norm, the most common of which is the Euclidean norm. This may be applied to the original dataset, or to a reduced dataset from SVD analysis. Based on the calculated distances, observations are grouped into clusters of similar

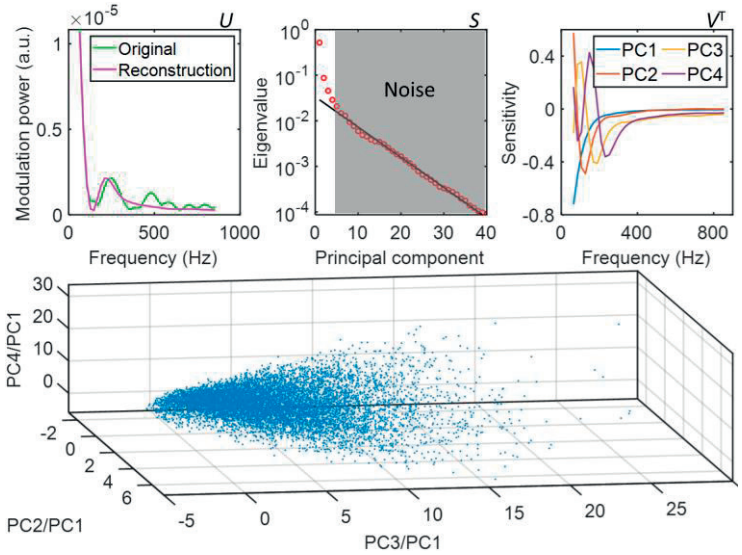

Figure 4.15 SVD factorization of the modulation spectra of insect observations. *The magnitude of the eigenvalues in S determines their relative importance. In this case, the first four principal components in V are included, and the rest are labelled as noise. The linear coefficients in U determine how much of each principal component is needed to reconstruct a given spectrum. Any modes observed in the scatter plot may correspond to different observed species or sexes of insects. Here, the original modulation spectrum is modelled with the four first principal components. Though the higher frequencies have lower magnitudes, it is known that they are important for classification. In this case it is evident that the first four principal components do not contain any high frequencies. The reconstruction only models the low-frequency part of the modulation spectrum, and no modes are observed in the scatterplot. The dataset may benefit from a more advanced method, such as HCA.*

observations in a dendrogram (Figure 4.16). HCA was used to distinguish male and female mosquitoes from other insects in Paper XII-XIII. Unsupervised methods are useful when there is no training data, such as the field implementations of entomological lidar carried out in this PhD work.

4.6.3. Supervised classification methods

Supervised classification methods utilize training data in which the classes of observations, such as the species and sexes of insects, are known in advance. The training data is used to construct a model by which the classes of unknown observations can be predicted. In the context of entomological lidar, supervised classification methods are difficult to implement due to the challenge involved in acquiring training data, i.e. releasing large numbers of classified insects into a laser beam propagating several meters above ground.

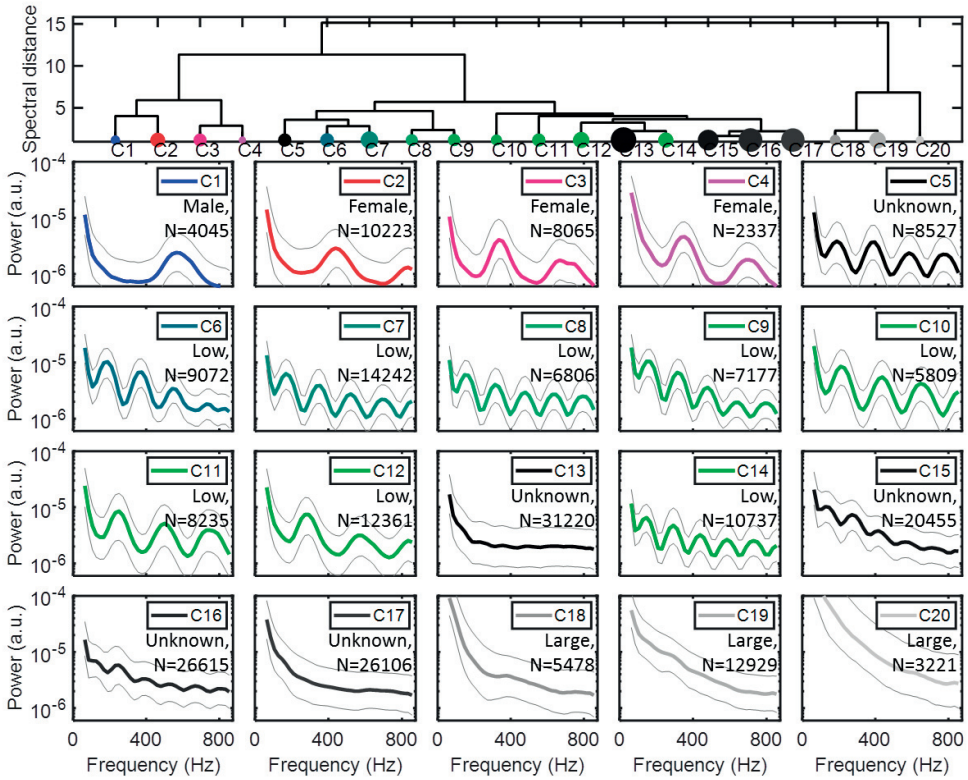

Figure 4.16 Dendrogram and clusters of insects based on Euclidean distance of their modulation spectra. *The dendrogram at the top shows how closely related the different clusters are, with three distinct groups of clusters emerging. Clusters 1-4 correspond to mosquitoes based on their high frequency contents. Clusters 5-17 contain a mix of low-frequency insects and unclassifiable observations, whereas clusters 18-20 contain observations corresponding to larger insects or vertebrates. The average spectrum, as well as minimum and maximum, are shown together with the number of observations in each cluster.*

Naïve Bayes classification (NBC) is a method in which Gaussian distributions are fitted to each observed parameter of each cluster of observations [136]. Each observation corresponds to a point in the parameter space, and new observations are classified based on proximity to the distributions from training data. The overlap between classes in the parameter space is used to evaluate the prediction accuracy of the acquired model. NBC was used in Paper II-III to classify mosquitoes based on their measured optical properties, and in Paper XII to evaluate the potential overlap of the obtained HCA clusters. NBC rely on two assumptions: that all observed parameters are independent, and that they can be modelled by a Gaussian distribution. It is unsuitable for classification based on modulation spectra due to the co-variance between wing-beat frequencies and their higher harmonics.

Regression is a statistical analysis tool in which one or more independent variables (predictors, $x=x_1,\ldots,x_n$) are used to estimate a dependent variable (outcome, y) [175]. This is done by finding the function F that best describes the relation between x and y. F is approximated by a polynomial according to Equation (4.16), which is written in matrix notation in Equation (4.17). The matrices X and K in Equation (4.17) are called the regressor matrix and the model matrix, respectively. The least squares solution to K is obtained through projection, see Equation (4.18).

$$y = F(x) \approx k_0 + k_1 x_1 + \ldots + k_n x_n \tag{4.16}$$

$$Y = [X_1^0 \; X_1^1 \; \ldots \; X_n^1] \begin{bmatrix} k_0 \\ k_1 \\ \vdots \\ k_n \end{bmatrix} = XK \tag{4.17}$$

$$K = (X^T X)^{-1} X^T Y \tag{4.18}$$

The model K can be obtained with a set of training data in which the outcome in known, and may thereafter be used to predict the outcome based on the predictors of new data. In this example, there was only a single outcome, and the model was linear. The same principle may be applied with two or more outcomes, modelled using second or higher order polynomials. Regression techniques are used in Paper II to obtain 3D flight coordinates, and in Paper V and VIII to parameterize insect wing beat harmonics. In case of high computational load due to large numbers of predictor variables, partial least squares (PLS) regression and linear discriminant analysis (LDA) are alternate methods in which the number of predictors is reduced in a process similar to PCA. Regression is then performed with the reduced set of predictors [176]. Artificial neural networks (ANN) are a related approach in which a network of artificial neurons with no prior knowledge is fed training data to learn how to distinguish target classes. ANNs have been demonstrated to be capable of classifying different species of insects [137].

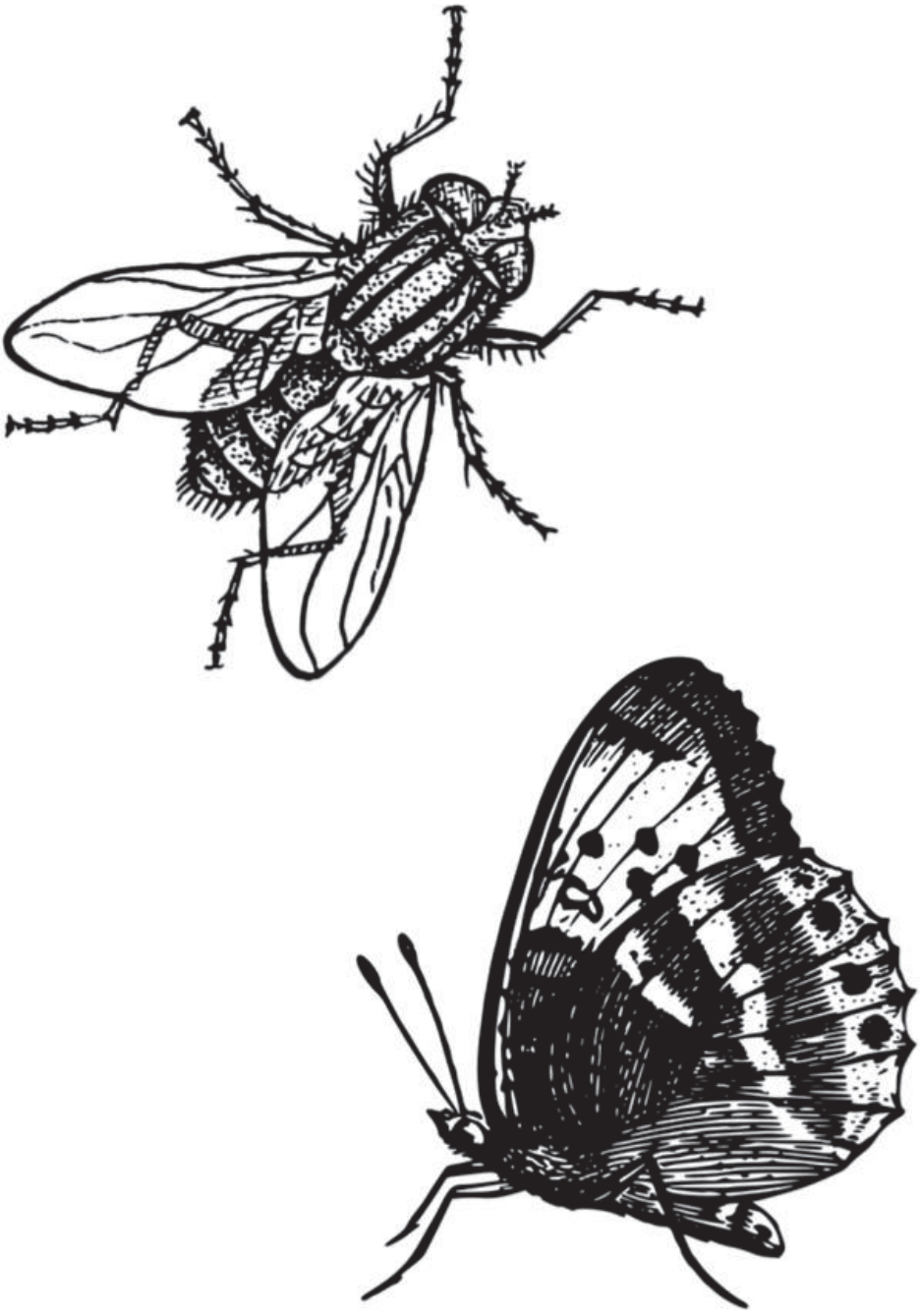

5. Conclusion and perspectives

Through the course of this PhD project, entomological lidar methods have been developed and improved in conjunction with data processing algorithms. Several lidar systems have been constructed and deployed in different field settings around the world, from boreal forest in Sweden, through different tropical settings in China, Tanzania and Ivory Coast, to a mountain top in Australia. Close to a million insects have been observed and characterized, and even more may be found in data sets that are yet to be evaluated. With field-sampling methods, such numbers of *in-situ* observations are inconceivable. Entomological radar can yield comparable numbers of observations [76], but radars are restricted to vertical implementations due to ground clutter. Thus, entomological lidar may provide researchers with data that is unattainable in other ways.

Entomological lidar is also significantly less intrusive than conventional methods, which typically involve catching and/or killing the study specimens. Whereas passive methods are fully non-intrusive, active laser-based methods may have slight effects on insects flying through the laser beam. Laser wavelengths that are invisible to insects are used [93, 156, 177]. However, the body may absorb some light which can lead to heating. When the laser is modulated on and off, this heating is periodic and may result in vibrations at the modulation frequency.

The usefulness of entomological lidar data relies on robust data processing and interpretation, as well as solid experimental design. Large amounts of data do not automatically equate to good data, after all. In this PhD project, a lot of effort has been put into the data processing. Each step in the process has been evaluated and improved, and alternative approaches have been developed and implemented when a method was found lacking. Further developments may include implementation of machine learning techniques for improved classification.

The optical properties of insects relate to physical properties, and through multiple spectral- or polarization bands, information on water contents, melanization, microstructures such as layered scales of Lepidoptera, body glossiness, wing glossiness and wing thickness may be obtained. In many cases, researchers are interested in the behavior of specific species and sexes, and laboratory investigation may yield information enabling the distinction of these species and sexes from other insects *in situ*. In some cases, entomological lidar systems may even be adapted and specialized based on the requirements of the study.

Entomological lidar technology continues being developed at a rapid pace. Through continuous hardware upgrades, the performance has been improved over the years. As in many other experimental designs, there is a tradeoff between sensitivity and sample rate – when one is increased, the other is reduced. High sensitivity enables detection of smaller organisms at farther ranges, whereas high sample rates enable the resolution of faster wing beats and more overtones which relate to the species and sexes of insects. Both are desired in the ideal case, but the specific requirements of a study may enable the reduction of one in favor of the other.

One drawback with entomological Scheimpflug lidar is that the alignment of the systems is a complex procedure that requires experience and technological knowledge. In addition, the optical and electronic components are sensitive to weather conditions. Thus, these systems require constant attendance by technologically knowledgeable personnel, which puts significant restraints on where, when and for how long measurements can be conducted. This may be improved by encapsulating and water proofing lidar systems, and remote control may even be an option. Such developments would increase the cost and complexity, but reduce the need for manpower.

Although so-called eye-safe laser wavelengths are selected, the laser output powers utilized in entomological Scheimpflug lidar makes eye safety a concern. Radiation legislation has to be considered when transmitting laser beams in free space, and a notice to airmen (NOTAM) may have to be issued in vertical implementations. The laser beams have propagated at least 3 m above ground consistently throughout this PhD project – this ensures eye-safe lidar operation, but makes intensity calibration more challenging.

The capability of entomological lidar as a research tool has reached a point where it may answer ecological questions. Laboratory reference data of focal species may inform decisions on design parameters of lidar systems. Quantitative information is obtained from each observed insect through rigorous data processing. Target classification enables detailed studies on the behavior of key insect groups, with implications for human health, economy and biodiversity. Though entomological lidar will never obtain information with the same level of detail as conventional field-sampling methods, the strengths of lidar complement the weaknesses of other methods excellently. Lidar measurements yield insect counts unattainable with other methods. With temporal- and spatial resolution in millisecond and centimeter scale, respectively, real-time data with detailed information on when, where and in which direction insects fly can be obtained.

At the onset of this PhD project in 2015, there were only a few groups pursuing electro-optical remote sensing of insects worldwide. Since then, the field has grown (Figure 5.1), and entomological optical remote sensing is now pursued

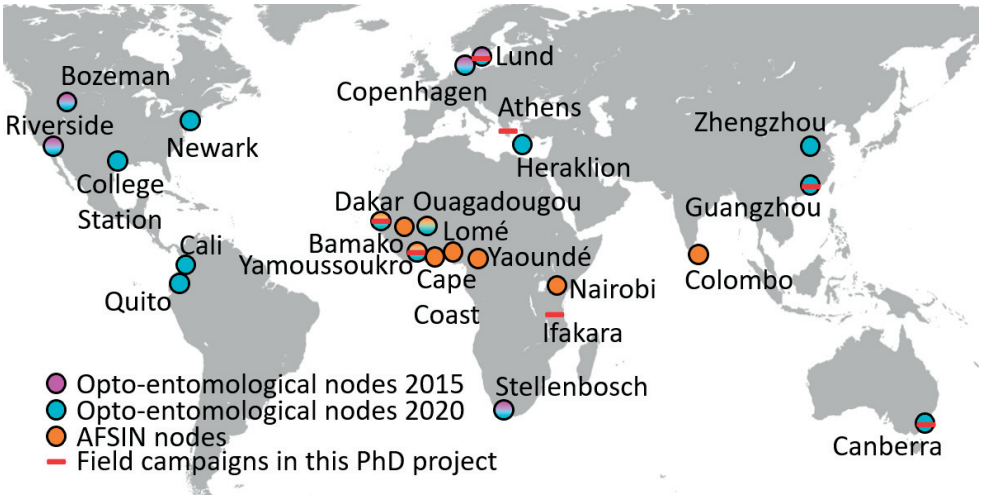

Figure 5.1 Entomological optical remote sensing world map. *The number of groups pursuing electro-optical remote sensing of insects has more than doubled in the past 5 years. Throughout this PhD work, field work has been carried out in a number of countries and locations, including collaborations with several AFSIN-affiliated research institutions.*

actively on all of Earth's continents apart from Antarctica. Although this PhD project has contributed to some of the growth, a lot has occurred independently of our group in Lund. One focus of this project has been tropical implementations in Africa in collaboration with the member institutions of the African spectral imaging network (AFSIN). This work has involved constructing optical remote sensing instruments and applying them to local problems, such as agricultural pests and disease vectors. The instrumentation has been donated to local research groups, which are now pursuing independent entomological lidar research.

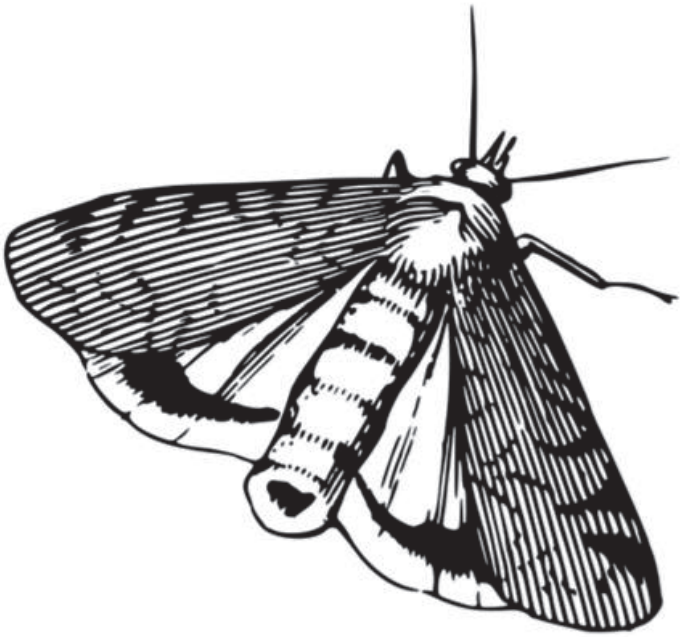

Acknowledgements

I would like to start by thanking my supervisor, *Mikkel Brydegaard*. I am very fortunate to have been given the opportunity to take part in such an interesting project, which has taken me all around the world! Despite being tough and difficult at times, it has been an amazing journey. Your combination of theoretical knowledge and practical skills is impressive, and you are always willing to share. I have learnt a lot from you, for which I am very thankful.

Joakim Bood, I am very happy to have had you as my co-supervisor on this project. Despite having a large workload, you have always been open for discussions and providing thoughtful feedback whenever needed.

To *Elin Malmqvist*, my partner in crime through most of this project. It really would not have been possible without you. We've been in all manner of strange situations and places together, and it's been so much fun! Your presence and involvement in playing with bugs is sorely missed.

To *Alem Gebru* and *Guangyu Zhao*, your presence and collaboration in the first half of this project was much appreciated. Through countless hours in the lab, discussions on measurements and data treatment, as well as cultural exchange at work and in private, we've had a lot of fun together! *Meng Li* and *Hampus Månefjord*, despite starting your projects relatively recently, you've already accomplished so much. With the two of you here, our little research group has doubled in size, and you've brought a lot of fun and inspiration to our weekly meetings.

I want to thank all of the students I have helped supervise – having the privilege to help and teach someone and watching them learn and grow is truly the biggest inspiration. *Mariam*, your cheerful attitude during long and cold nights in the lab was impressive, and I am very fortunate to have been able to supervise your work. *Alexandra*, thanks for the good times in Côte d'Ivoire. The trip was truly an adventure, including robbery attempts and our equipment being wrecked by a storm. Hasa diga Eebowai. Despite this, we managed to pull through and have a good time! Thanks to *Klas* and *Alfred* for your enthusiasm and self-sufficiency – I'm inspired and impressed by the work you do nowadays! *Peggy*, thanks for good times in the lab. *Jonathan*, you always bring a positive vibe, and I look forward to your thesis defense tomorrow (at the time of writing)! *Martin* and *Ludvig*, your

joint project has been interesting to follow, and I look forward to seeing its conclusion.

I want to thank *Susanne Åkesson* for all the interesting opportunities for field campaigns with LUMBO. It is always a joy to discuss ideas and results with you. *Jens Rydell*, your endless enthusiasm is an inspiration, and working together with you is never dull! Thanks also to *Carsten Kirkeby*, *Rickard Ignell*, *Gerry Killeen*, *Fredros Okumu*, *Yeromin Mlacha*, *Sarah Moore*, *Anna Runemark* and *Jessica Abbott* for fruitful discussion and collaboration, and providing the ecological perspective. It has been a great joy to be able to learn so much from experts in an adjacent research field.

Jérémie Zoueu, you were a gracious host in Côte d'Ivoire, and just as gracious during your visits in Lund. Collaborating with you has been a joy, and I'm so happy that you're attending my thesis defense. *Benoit Kouakou*, doing lidar measurements with has been a pleasure! Great job on your manuscript. *Alvarez Kossonou*, it was fun having you here in Sweden for some time, and even more fun meeting you again in Senegal and Côte d'Ivoire. *Moussa Sougoti*, it's been a joy seeing how the idea you got during a conversation in Senegal turned into experiments and a manuscript. It's very interesting work! Thanks to *Amadou Wague*, *Fatou Gueye*, *Fatou Ndoi*, *Modou Mbaye* and everyone else for hosting us and doing experiments together in Senegal. I also want to thank everyone else in *AFSIN*, it's been so interesting to get to know you and your work all over Africa. I especially want to thank *Ernst van Groningen*, *Carla Puglia* and *Therese Rantakokko* for making it all possible through the ISP programme in Uppsala. *Aboma Merdasa* and *Edouard Berrocal*, thanks for all the banter during and after the AFSIN workshop in Dakar.

Thanks to *Sune Svanberg* for your positive and cheerful demeanor at all times. It is infectious, and one cannot help but be inspired. Thanks also to *Katarina Svanberg*, *Shiming Zhu*, *Yiyun Li*, *Wansha Li*, *Zheng Duan*, *Hongqiang Feng*, *Ziwei Song* and everyone else who participated in the field campaign in Guangzhou. It was a great experience despite the very hot and humid weather.

I want to thank *Eric Warrant*, *Anna Honkanen*, *David Dreyer*, *Jesse Amenuvegbe Wallace* and *Gabriel Gabiru* for great times in the cabin in Australia. The thought of flesh-eating kangaroos gives me nightmares to this day. I look forward to working more together in the future.

Jord Prangsma, *Josefine Holm Nielsen* and everyone else currently or previously affiliated with *Fauna Photonics*, thank you for doing such interesting things across the bridge! I always enjoy our meetings and discussions. *Alexandros Papayannis* and *Georgios Tsaknakis*, thank you for good lidar discussions and collaboration early on in this PhD project.

Marcus Aldén, thank you for leading our division all this time. It's clear to me that you have your heart in the right place, which I think is a crucial trait for a leader. You have really constructed a good social environment at our workplace, and I believe that this facilitates collaboration and pays dividends in the research activities as well. *Minna*, *Cecilia* and *Igor*, you are the heart of this division. Without you around, the rest of us would be lost and helpless. You also do a lot for the friendly atmosphere we have, which is appreciated by everyone. Thank you.

I want to thank my friends at the division. *Joakim*, thanks for being my office mate all this time. I find it amazing that we still haven't thrown out the old junk that was lying around when we first moved in, but just shoved it into a corner and left it for five years. It's equally amazing that the plant has survived for so long. Thanks to *Jim* for our painting sessions, to *Kajsa* for always having a ruler at hand, to *Christopher* for writing books for me, to *Adrian*, *Maria*, *Haisol*, *Torsten*, *Dina*, *Simon* and others for good times at the climbing gym, to *Manu* and *Xin* for saving me in December, to *Arman*, *Marco*, *Henrik*, *Panagiota*, *Alexios*, *Fahed*, *Saeed*, etc… The list is too long to write here. To all of you, it's been a joy to be your colleague.

Finally, I want to thank the people that are most important to me. *Mom* and *dad*, thank you for supporting me through all these years, and for being there whenever I needed you. It means so much to me. *Robin*, my dear brother, thank you for being such a bastard (or wait, I guess technically I am the bastard)! It's funny that we're both finishing our academic studies at the same time, and are even writing our final essays at the same time! Best of luck to us both. To my sambo *Nelly*, thank you for bringing a lot of fun and silly ideas into my life. You give me new perspectives on life every single day. I also want to thank you for putting up with me while writing my thesis – it can't have been easy, and I hope to be able to return the favor one day. To all my *friends* and *relatives*, from the bottom of my heart, thank you for being there. Without you, I really wouldn't have gotten to where I am today.

Funding

This research was made possible through the support from a number of funding organizations and foundations, for which I am very thankful.

The Swedish Research Council through a U-Forsk grant and Linnaeus grants to the Lund Laser Centre (LLC) and the Center for Animal Movement Research (CAnMove).

The Royal Physiographic Society of Lund.

The Swedish Energy Agency.

Innovationsfonden DK.

The International Science Program (ISP).

The African Spectral Imaging Network (AFSIN).

FORMAS.

References

1. Rizvić, S., et al. *LiDAR based terrains for virtual cultural heritage applications*. in *2014 X International Symposium on Telecommunications (BIHTEL)*. 2014.
2. Wulder, M.A., et al., *Lidar sampling for large-area forest characterization: a review.* Remote Sensing of Environment, 2012. **121**: p. 196-209.
3. Schwarz, B., *Lidar: Mapping the world in 3D.* Nature Photonics, 2010. **4**(7): p. 429-430.
4. Lenoble, J., L. Remer, and D. Tanré, *Aerosol remote sensing*. 2013, Berlin; New York: Springer.
5. Papayannis, A., et al., *Systematic lidar observations of Saharan dust over Europe in the frame of EARLINET (2000–2002).* Journal of Geophysical Research: Atmospheres, 2008. **113**.
6. Fujii, T.D. and T. Fukuchi, *Laser remote sensing.* Optical engineering: 97. 2005: Boca Raton : Taylor & Francis, 2005.
7. Papayannis, A., et al., *Multiwavelength lidar for ozone measurements in the troposphere and the lower stratosphere.* Applied Optics, 1990. **29**(4): p. 467.
8. Elterman, L., *Aerosol Measurements in the Troposphere and Stratosphere.* Applied Optics, 1966. **5**(11): p. 1769-1776.
9. Shaw, J.A., et al., *Polarization lidar measurements of honey bees in flight for locating land mines.* Optics Express, 2005. **13**(15): p. 5853-5863.
10. Brydegaard, M., et al., *Insect monitoring with fluorescence lidar techniques: feasibility study.* Applied Optics, 2009. **48**(30): p. 5668.
11. Repasky, K.S., et al., *Optical detection of honeybees by use of wing-beat modulation of scattered laser light for locating explosives and land mines.* Applied Optics, 2006. **45**(8): p. 1839.
12. Brydegaard, M., A. Gebru, and S. Svanberg, *Super Resolution Laser Radar with Blinking Atmospheric Particles - Application to Interacting Flying Insects.* Progress in Electromagnetics Research, 2014. **147**: p. 141-151.
13. Brydegaard, M. and S. Svanberg, *Photonic Monitoring of Atmospheric and Aquatic Fauna.* Laser & Photonics Reviews, 2018. **12**: p. 1800135.

14. Potamitis, I. and I. Rigakis, *Large Aperture Optoelectronic Devices to Record and Time-Stamp Insects Wingbeats.* IEEE Sensors Journal, 2016. **16**(15): p. 6053-6061.
15. Zhao, G., et al., *Inelastic hyperspectral lidar for profiling aquatic ecosystems.* Laser & Photonics Reviews, 2016. **10**.
16. Nielsen, J.H., et al., *Investigation of autofluorescence in zooplankton for use in classification of larval salmon lice.* Applied Optics, 2019. **58**(26): p. 7022-7027.
17. Jacques, S.L., *Optical properties of biological tissues: a review.* Phys Med Biol, 2013. **58**(11): p. R37-61.
18. de Boer, J.F., C.K. Hitzenberger, and Y. Yasuno, *Polarization sensitive optical coherence tomography; a review.* Biomedical Optics Express, 2017. **8**(3): p. 1838-1873.
19. Konugolu Venkata Sekar, S., et al., *Solid phantom recipe for diffuse optics in biophotonics applications: A step towards anatomically correct 3D tissue phantoms.* Biomedical Optics Express, 2019. **10**: p. 2090.
20. Genoud, A.P., et al., *Identification of gravid mosquitoes from changes in spectral and polarimetric backscatter cross sections.* 2019. **12**(10): p. e201900123.
21. Drake, V.A. and D.R. Reynolds, *Radar entomology: Observing insect flight and migration*. 2012: CABI Publishing. 1-489.
22. Chapman, J.W., D.R. Reynolds, and A.D. Smith, *Vertical-Looking Radar: A New Tool for Monitoring High-Altitude Insect Migration.* BioScience, 2003. **53**(5): p. 503-511.
23. Zaugg, S., et al., *Automatic identification of bird targets with radar via patterns produced by wing flapping.* Journal of the Royal Society Interface, 2008. **5**(26): p. 1041-1053.
24. Shamoun-Baranes, J., et al., *Taking radar Aeroecology into the 21st century.* Ecography, 2019. **42**.
25. Chilson, P.B., et al., *Radar aeroecology: exploring the movements of aerial fauna through radio-wave remote sensing.* Biology Letters, 2012. **8**.
26. Lin, T.-Y., et al., *MistNet: Measuring historical bird migration in the US using archived weather radar data and convolutional neural networks.* Methods in Ecology and Evolution, 2019.
27. Nilsson, C., et al., *Revealing patterns of nocturnal migration using the European weather radar network.* Ecography, 2018.
28. Drake, V.A., *Distinguishing target classes in observations from vertically pointing entomological radars.* International Journal of Remote Sensing, 2016. **37**(16): p. 3811-3835.
29. Smith, A.D., J.R. Riley, and R.D. Gregory, *A method for routine monitoring of the aerial migration of insects by using a vertical-looking radar.* Philosophical Transactions of the Royal Society of London. Series B: Biological Sciences, 1993. **340**(1294): p. 393-404.

30. Malanowski, M., *Influence of integration time on tracking performance in PCL radar*. Photonics Applications in Astronomy, Communications, Industry, and High-Energy Physics Experiments 2007. Vol. 6937. 2007: SPIE.
31. Gao, Y.B., et al., *Dynamic analysis on the migration of the rice leaf roller Cnaphalocrocis medinalis (Lepidoptera: Pyralidae) by Doppler Insect Monitoring Radar and numerical simulation.* Shengtai Xuebao/ Acta Ecologica Sinica, 2008. **28**: p. 5238-5247.
32. Britch, S., et al., *Acoustic Control of Mosquito Larvae In Artificial Drinking Water Containers.* Journal of the American Mosquito Control Association, 2016. **32**: p. 341-344.
33. Mitson, R.B., *Review of high-speed sector-scanning sonar and its application to fisheries research.* IEE Proceedings F - Communications, Radar and Signal Processing, 1984. **131**(3): p. 257-269.
34. Hertz, C.H., *Untersuchung spezieller Formen der Koronaentladung an Spitzen und Drähten*. 1955, Lund.
35. Arnett, E.B., et al., *Evaluating the Effectiveness of an Ultrasonic Acoustic Deterrent for Reducing Bat Fatalities at Wind Turbines.* PLOS ONE, 2013. **8**(6): p. e65794.
36. Ganchev, T., *Computational Bioacoustics*. 2017: De Gruyter.
37. Sandsten, M. and J. Brynolfsson. *Classification of bird song syllables using Wigner-Ville ambiguity function cross-terms*. in *2017 25th European Signal Processing Conference (EUSIPCO)*. 2017.
38. Wilson, D., et al., *Sound Finder: A new software approach for localizing animals recorded with a microphone array.* Bioacoustics, 2013. **23**.
39. Vasconcelos, D., et al. *LOCOMOBIS: a low-cost acoustic-based sensing system to monitor and classify mosquitoes*. in *2019 16th IEEE Annual Consumer Communications & Networking Conference (CCNC)*. 2019.
40. Mukundarajan, H., et al., *Using mobile phones as acoustic sensors for high-throughput mosquito surveillance.* eLife, 2017. **6**: p. e27854.
41. Silver, J.B., *Mosquito Ecology: Field Sampling Methods*. 2008: Springer.
42. Bidlingmayer, W.L., *Use of the truck trap for evaluating adult mosquito populations.* Mosquito News, 1966. **26**(2): p. 139-143.
43. Schlyter, F., J. Byers, and J. Löfqvist, *Attraction to pheromone sources of different quantity, quality, and spacing: Density-regulation mechanisms in bark beetle Ips typographus.* Journal of chemical ecology, 1987. **13**: p. 1503-23.
44. Kirkeby, C., et al., *Quantifying dispersal of european culicoides (Diptera: Ceratopogonidae) vectors between farms using a novel mark-release-recapture technique.* PLoS One, 2013. **8**(4): p. e61269.
45. Egri, Á., et al., *Polarotactic tabanids find striped patterns with brightness and/or polarization modulation least attractive: an advantage of zebra stripes.* The Journal of Experimental Biology, 2012. **215**(5): p. 736-745.

46. Huestis, D., et al., *Windborne long-distance migration of malaria mosquitoes in the Sahel.* Nature, 2019. **574**: p. 404-408.
47. Wellenreuther, M., et al., *Environmental and Climatic Determinants of Molecular Diversity and Genetic Population Structure in a Coenagrionid Damselfly.* PLOS ONE, 2011. **6**(6): p. e20440.
48. Chetverikov, P., *Confocal laser scanning microscopy technique for the study of internal genitalia and external morphology of eriophyoid mites (Acari: Eriophyoidea).* Zootaxa, 2012. **3453**(1).
49. Engel, S., et al., *The use of tunable diode laser absorption spectroscopy for rapid measurements of the delta13C of animal breath for physiological and ecological studies.* Rapid Commun Mass Spectrom, 2009. **23**(9): p. 1281-6.
50. IAEA, *Manual for the Use of Stable Isotopes in Entomology*. 2009, Vienna: International Atomic Energy Agency.
51. World Health Organization, *World Malaria Report*. 2017.
52. Murray, C.J.L., et al., *Global malaria mortality between 1980 and 2010: a systematic analysis.* The Lancet, 2012. **379**(9814): p. 413-431.
53. Sachs, J. and P. Malaney, *The economic and social burden of malaria.* Nature, 2002. **415**(6872): p. 680-5.
54. Kiszewski, A., et al., *A global index representing the stability of malaria transmission.* Am J Trop Med Hyg, 2004. **70**(5): p. 486-98.
55. Killeen, G.F., *Characterizing, controlling and eliminating residual malaria transmission.* Malaria Journal, 2014. **13**(1): p. 330.
56. Bhatt, S., et al., *The effect of malaria control on Plasmodium falciparum in Africa between 2000 and 2015.* Nature, 2015. **526**: p. 207.
57. Gething, P.W., et al., *Mapping Plasmodium falciparum Mortality in Africa between 1990 and 2015.* New England Journal of Medicine, 2016. **375**(25): p. 2435-2445.
58. Moiroux, N., et al., *Changes in Anopheles funestus Biting Behavior Following Universal Coverage of Long-Lasting Insecticidal Nets in Benin.* The Journal of Infectious Diseases, 2012. **206**(10): p. 1622-1629.
59. Alonso, P. and A.M. Noor, *The global fight against malaria is at crossroads.* The Lancet, 2017. **390**(10112): p. 2532-2534.
60. Ferguson, H.M., et al., *Ecology: A Prerequisite for Malaria Elimination and Eradication.* PLOS Medicine, 2010. **7**(8): p. e1000303.
61. Oliveira, C.M., et al., *Crop losses and the economic impact of insect pests on Brazilian agriculture.* Crop Protection (02612194), 2014. **56**: p. 50.
62. Das, A.J., N.L. Stephenson, and K.P. Davis, *Why do trees die? Characterizing the drivers of background tree mortality.* Ecology, 2016. **97**(10): p. 2616-2627.
63. Göthlin, E., L.M. Schroeder, and A. Lindelöw, *Attacks by Ips typographus and Pityogenes chalcographus on Windthrown Spruces (Picea abies)*

During the Two Years Following a Storm Felling. Scandinavian Journal of Forest Research, 2000. **15**(5): p. 542-549.
64. Fleming, R. and J.-N. Candau, *Influences of Climatic Change on Some Ecological Processes of an Insect Outbreak System in Canada's Boreal Forests and the Implications for Biodiversity.* Environmental Monitoring and Assessment, 1998. **49**: p. 235-249.
65. Vrijheid, M., et al., *Review: Environmental pollutants and child health—A review of recent concerns.* International Journal of Hygiene and Environmental Health, 2016. **219**: p. 331-342.
66. Zhao, K.-F., Z.-P. Shi, and J.-C. Wu, *Insecticide-induced enhancement of flight capacity of the brown planthopper Nilaparvata lugens Stål (Hemiptera: Delphacidae).* Crop Protection, 2011. **30**(4): p. 476-482.
67. Cheng, Y., et al., *Possible connection between imidacloprid-induced changes in rice gene transcription profiles and susceptibility to the brown plant hopper Nilaparvata lugens Stål (Hemiptera: Delphacidae).* Pesticide Biochemistry and Physiology, 2012. **102**(3): p. 213-219.
68. Wang, L.-P., et al., *Insecticide-induced increase in the protein content of male accessory glands and its effect on the fecundity of females in the brown planthopper Nilaparvata lugens Stål (Hemiptera: Delphacidae).* Crop Protection, 2010. **29**(11): p. 1280-1285.
69. Potamitis, I., et al., *In-Vivo Vibroacoustic Surveillance of Trees in the Context of the IoT.* Sensors, 2019. **19**: p. 1366.
70. Ashman, T.-L., et al., *Pollen limitation of plant reproduction: ecological and evolutionary causes and consequences.* Ecology, 2004. **85**(9): p. 2408-2421.
71. Klein, A.-M., et al., *Importance of pollinators in changing landscapes for world crops.* Proceedings of the Royal Society B: Biological Sciences, 2007. **274**(1608): p. 303-313.
72. Potts, S.G., et al., *Global pollinator declines: trends, impacts and drivers.* Trends Ecol Evol, 2010. **25**(6): p. 345-53.
73. Smith, M.R., et al., *Effects of decreases of animal pollinators on human nutrition and global health: a modelling analysis.* The Lancet, 2015. **386**: p. 1964-1972.
74. Ekroos, J., et al., *High land-use intensity in grasslands constrains wild bee species richness in Europe.* Biological Conservation, 2020. **241**: p. 108255.
75. Sánchez-Bayo, F., et al., *Are bee diseases linked to pesticides? — A brief review.* Environment International, 2016. **89**: p. 7-11.
76. Hu, G., et al., *Mass seasonal bioflows of high-flying insect migrants.* Science, 2016. **354**(6319): p. 1584-1587.
77. Newton, I. and K. Brockie, *The migration ecology of birds*. 2008: Amsterdam ; London : Academic Press.

78. Dreyer, D., et al., *Evidence for a southward autumn migration of nocturnal noctuid moths in central Europe.* The Journal of Experimental Biology, 2018. **221**: p. jeb179218.
79. Dreyer, D., et al., *The Earth's Magnetic Field and Visual Landmarks Steer Migratory Flight Behavior in the Nocturnal Australian Bogong Moth.* Current Biology, 2018. **28**(13): p. 2160-2166.e5.
80. Reed, K.D., et al., *Birds, migration and emerging zoonoses: west nile virus, lyme disease, influenza A and enteropathogens.* Clin Med Res, 2003. **1**(1): p. 5-12.
81. Cox, G.W., *Bird Migration and Global Change*. 2010, Washington, DC: Island Press.
82. Green, K., et al., *The Australian Bogong moth (Agrotis infusa, Lepidoptera: Noctuidae) 1951-2020: Decline and crash.* Austral Entomology, submitted.
83. Common, I.F.B., *Migration and Gregarious Æstivation in the Bogong Moth, Agrotis infusa.* Nature, 1952. **170**(4336): p. 981-982.
84. Hespenheide, H., *Selective predation by two swifts and a swallow in Central America.* Ibis, 2008. **117**: p. 82-99.
85. Collins, C.T. and B.T. Thomas, *Food Habits of Two Fork-tailed Swifts in Venezuela.* The Wilson Journal of Ornithology, 2012. **124**(1): p. 152-157, 6.
86. Rydell, J., J. Eklöf, and S. Sánchez-Navarro, *Age of enlightenment: long-term effects of outdoor aesthetic lights on bats in churches.* Royal Society open science, 2017. **4**(8): p. 161077-161077.
87. Rydell, J., et al., *Effects of wind power on birds and bats - An updated synthesis report*. 2017: Naturvårdsverket.
88. Sánchez-Navarro, S., J. Rydell, and C. Ibáñez, *Bat fatalities at wind-farms in the lowland Mediterranean of southern Spain.* Acta Chiropterologica, 2019: p. under review.
89. Zimmerling, J.R. and C.M. Francis, *Bat mortality due to wind turbines in Canada.* The Journal of Wildlife Management, 2016. **80**(8): p. 1360-1369.
90. Hayes, M.A., *Bats Killed in Large Numbers at United States Wind Energy Facilities.* BioScience, 2013. **63**(12): p. 975-979.
91. Voigt, C.C., et al., *The catchment area of wind farms for European bats: A plea for international regulations.* Biological Conservation, 2012. **153**: p. 80-86.
92. Tedore, C. and D.-E. Nilsson, *Avian UV vision enhances leaf surface contrasts in forest environments.* Nature Communications, 2019. **10**(1): p. 238.
93. Cronin, T.W., et al., *Visual Ecology*. 2014: Princeton University Press.
94. Rashed, R., *A Pioneer in Anaclastics: Ibn Sahl on Burning Mirrors and Lenses.* Isis, 1990. **81**(3): p. 464-491.
95. Newton, I., *Lectiones Opticae.* 1669.

96. Robinson, A., *The Last Man Who Knew Everything: Thomas Young, The Anonymous Polymath Who Proved Newton Wrong, Explained How We See, Cured the Sick, and Deciphered the Rosetta Stone, Among Other Feats of Genius*. 2006: New York: Pi Press.
97. Ashkin, A., J.M. Dziedzic, and T. Yamane, *Optical trapping and manipulation of single cells using infrared laser beams.* Nature, 1987. **330**(6150): p. 769-771.
98. Pesce, G., et al., *Step-by-step guide to the realization of advanced optical tweezers.* Journal of the Optical Society of America B, 2015. **32**(5): p. B84-B98.
99. Koch, G., et al., *High-energy 2 μm Doppler lidar for wind measurements.* Optical Engineering, 2007. **46**(11): p. 116201.
100. Walther, J., et al., *Optical coherence tomography in biomedical research.* Anal Bioanal Chem, 2011. **400**(9): p. 2721-43.
101. Jacques, S., *Polarized Light Imaging of Biological Tissues*, in *Handbook of Biomedical Optics*, D. Boas, C. Pitris, and N. Ramanujam, Editors. 2011, CRC Press.
102. Arwin, H., et al., *Chirality-induced polarization effects in the cuticle of scarab beetles: 100 years after Michelson.* Philosophical Magazine, 2012. **92**(12): p. 1583-1599.
103. Nixon, M.R., A.G. Orr, and P. Vukusic, *Wrinkles enhance the diffuse reflection from the dragonfly Rhyothemis resplendens.* Journal of The Royal Society Interface, 2015. **12**(103): p. 20140749.
104. Shevtsova, E., et al., *Stable structural color patterns displayed on transparent insect wings.* Proceedings of the National Academy of Sciences, 2011. **108**(2): p. 668-673.
105. Miles, R.B., W.R. Lempert, and J.N. Forkey, *Laser Rayleigh scattering.* Measurement Science and Technology, 2001. **12**(5): p. R33-R51.
106. Mishchenko, M.I., L.D. Travis, and A.A. Lacis, *Scattering, Absorption and Emission of Light By Small Particles*. 2002: Cambridge university press.
107. Bohren, C.F. and D.R. Huffman, *Absorption and Scattering of Light by Small Particles*. 1998: WILEY-VCH Verlag GmbH & Co. KGaA.
108. Tomasi, C., et al., *Aerosol remote sensing in polar regions.* Earth-Science Reviews, 2015. **140**: p. 108-157.
109. Stavenga, D.G., *Thin Film and Multilayer Optics Cause Structural Colors of Many Insects and Birds.* Materials Today: Proceedings, 2014. **1**: p. 109-121.
110. Backman, V., et al., *Polarized light scattering spectroscopy for quantitative measurement of epithelial cellular structures in situ.* IEEE Journal of Selected Topics in Quantum Electronics, 1999. **5**(4): p. 1019-1026.

111. Shawkey, M.D., et al., *Electron tomography, three-dimensional Fourier analysis and colour prediction of a three-dimensional amorphous biophotonic nanostructure.* Journal of The Royal Society Interface, 2009. **6**(suppl_2): p. S213-S220.
112. Seago, A.E., et al., *Gold bugs and beyond: a review of iridescence and structural colour mechanisms in beetles (Coleoptera).* J R Soc Interface, 2009. **6 Suppl 2**: p. S165-84.
113. Pirih, P., B. Wilts, and D. Stavenga, *Spatial reflection patterns of iridescent wings of male pierid butterflies: Curved scales reflect at a wider angle than flat scales.* Journal of comparative physiology. A, Neuroethology, sensory, neural, and behavioral physiology, 2011. **197**: p. 987-97.
114. Vukusic, P., J.R. Sambles, and C.R. Lawrence, *Structurally assisted blackness in butterfly scales.* Proceedings of the Royal Society of London. Series B: Biological Sciences, 2004. **271**(suppl_4): p. S237-S239.
115. Yin, H., et al., *Iridescence in the neck feathers of domestic pigeons.* Phys Rev E Stat Nonlin Soft Matter Phys, 2006. **74**(5 Pt 1): p. 051916.
116. Prum, R.O. and R. Torres, *Structural colouration of avian skin: convergent evolution of coherently scattering dermal collagen arrays.* J Exp Biol, 2003. **206**(Pt 14): p. 2409-29.
117. Saleh, B.E.A. and M.C. Teich, *Fundamentals of photonics*. 2007: Hoboken, N.J. : Wiley.
118. Pena, A.M., et al., *Spectroscopic analysis of keratin endogenous signal for skin multiphoton microscopy: erratum.* Optics Express, 2005. **13**(17): p. 6667-6667.
119. Bendit, E.G. and D. Ross, *A Technique for Obtaining the Ultraviolet Absorption Spectrum of Solid Keratin.* Applied Spectroscopy, 1961. **15**(4): p. 103-105.
120. Perna, G., et al., *Fluorescence spectroscopy of synthetic melanin in solution.* Journal of Luminescence, 2009. **129**(1): p. 44-49.
121. Jacques, S., R. Glickman, and J. Schwartz, *Internal absorption coefficient and threshold for pulsed laser disruption of melanosomes isolated from retinal pigment epithelium*. Photonics West '96. Vol. 2681. 1996: SPIE.
122. Burresi, M., et al., *Bright-White Beetle Scales Optimise Multiple Scattering of Light.* Scientific Reports, 2014. **4**(1): p. 6075.
123. Jacques, S.L. and B.W. Pogue, *Tutorial on diffuse light transport.* J Biomed Opt, 2008. **13**(4): p. 041302.
124. Jacques, S.L. and L. Wang, *Monte Carlo Modeling of Light Transport in Tissues*, in *Optical-Thermal Response of Laser-Irradiated Tissue*. 1995, Springer, Boston, MA. p. R37-61.
125. Berrocal, E. and J. Jönsson, *Development of future spray imaging techniques using General Purpose GPU accelerated Monte Carlo simulation*. 2012.

126. Mishchenko, M.I. and L.D. Travis, *Polarization and Depolarization of Light*, in *Light Scattering from Microstructures*. 2000, Springer.
127. Liechti, F., B. Bruderer, and P. Heidi, *Quantification of Nocturnal Bird Migration by Moonwatching: Comparison with Radar and Infrared Observations (Cuantificación de la Migración Nocturna de Aves Observando la Luna: Comparación con Observaciones de Radar e Intrarrojas)*. 1995, Association of Field Ornithologists, Inc. p. 457.
128. Lundin, P., et al. *Passive unmanned sky spectroscopy for remote bird classification*. 2011.
129. Runemark, A., et al., *Rare Events in Remote Dark-Field Spectroscopy: An Ecological Case Study of Insects.* JSTQE, 2012. **18**(5): p. 1573-1582.
130. Lundin, P., et al., *Remote nocturnal bird classification by spectroscopy in extended wavelength ranges.* Applied Optics, 2011. **50**(20): p. 3396-3411.
131. Park, Y., et al., *Fabrication and Characterization of a GaN Light-emitting Diode (LED) with a Centered Island Cathode.* Journal of the Optical Society of Korea, 2012. **16**.
132. Donati, S. and F. Montecchi, *Analysis of frequency response and noise of CCD structures.* Revue de Physique Appliquee, 1978. **13**(12): p. 691-696.
133. Randeberg, L. and J. Hernandez-Palacios, *Hyperspectral imaging of bruises in the SWIR spectral region*. SPIE BiOS. Vol. 8207. 2012: SPIE.
134. Riley, J.R., *Angular and temporal variations in the radar cross-sections of insects.* Proceedings of the Institution of Electrical Engineers, 1973. **120**(10): p. 1229-1232.
135. Nguyen, C.V., et al., *Capturing Natural-Colour 3D Models of Insects for Species Discovery and Diagnostics.* PLOS ONE, 2014. **9**(4): p. e94346.
136. Chen, Y., et al., *Flying Insect Classification with Inexpensive Sensors.* Journal of Insect Behavior, 2014. **27**(5): p. 657-677.
137. Moore, A. and R.H. Miller, *Automated Identification of Optically Sensed Aphid (Homoptera: Aphidae) Wingbeat Waveforms.* Annals of the Entomological Society of America, 2002. **95**(1): p. 1-8.
138. Potamitis, I. and I. Rigakis, *Novel Noise-Robust Optoacoustic Sensors to Identify Insects Through Wingbeats.* IEEE Sensors Journal, 2015. **15**(8): p. 4621-4631.
139. Potamitis, I. and I. Rigakis, *Measuring the fundamental frequency and the harmonic properties of the wingbeat of a large number of mosquitoes in flight using 2D optoacoustic sensors.* Applied Acoustics, 2016. **109**: p. 54-60.
140. Dell, A.I., et al., *Automated image-based tracking and its application in ecology.* Trends in Ecology & Evolution, 2014. **29**(7): p. 417-428.
141. Hein, A., et al., *Conserved behavioral circuits govern high-speed decision-making in wild fish shoals.* Proceedings of the National Academy of Sciences, 2018. **115**: p. 201809140.

142. Bomphrey, R.J., et al., *Smart wing rotation and trailing-edge vortices enable high frequency mosquito flight.* Nature, 2017. **544**(7648): p. 92-95.
143. Brydegaard, M., et al., *Realistic Instrumentation Platform for Active and Passive Optical Remote Sensing.* Applied Spectroscopy, 2015: p. in press.
144. Gebru, A., et al., *Investigation of atmospheric insect wing-beat frequencies and iridescence features using a multi-spectral kHz remote detection system.* Journal of Applied Remote Sensing, 2014. **9221**: p. 922106-922106-17.
145. Edrich, M., S. Lutz, and F. Hoffmann. *Passive Radar at Hensoldt: A Review to the last Decade*. in *2019 20th International Radar Symposium (IRS)*. 2019.
146. Schroeder, A., M. Edrich, and V. Winkler, *Multi-Illuminator Passive Radar Performance Evaluation.* 2012: p. 61-64.
147. Mei, L. and M. Brydegaard, *Atmospheric aerosol monitoring by an elastic Scheimpflug lidar system.* Optics Express, 2015. **23**(24): p. A1613-A1628.
148. Mayer, H., *Theodor Scheimpflug.* Ophthalmic Research, 1994. **26(suppl 1)**(Suppl. 1): p. 3-9.
149. Malmqvist, E., *From Fauna to Flames - Remote Sensing with Scheimpflug Lidar*, PhD thesis, LRCP-218, Lund University, 2019.
150. Jansson, S., et al., *Exploitation of an atmospheric lidar network node in single-shot mode for the classification of aerofauna.* Journal of Applied Remote Sensing, 2017. **11**(3): p. 1-14, 14.
151. Mei, L., et al., *Comparison studies of the Scheimpflug lidar technique and the pulsed lidar technique for atmospheric aerosol sensing.* Appl Opt, 2019. **58**(32): p. 8981-8992.
152. Malmqvist, E., et al., *Scheimpflug Lidar for combustion diagnostics.* Optics Express, 2018. **26**(12): p. 14842-14858.
153. Larsson, J., et al., *Atmospheric CO2 sensing using Scheimpflug-lidar based on a 1.57-μm fiber source.* Optics Express, 2019. **27**(12): p. 17348-17358.
154. Wang, X., et al., *Drone-based area scanning of vegetation fluorescence height profiles using a miniaturized hyperspectral lidar system.* Applied Physics B, 2018. **124**(11): p. 207.
155. Song, Z., et al., *Application of lidar remote sensing of insects in agricultural entomology on the Chinese scene.* Journal of Applied Entomology, in print, 2019.
156. Brydegaard, M., et al., *Short-Wave infrared atmospheric scheimpflug lidar.* EPJ Web Conf., 2018. **176**: p. 01012.
157. Hooper, W.P. and G.M. Frick, *Lidar detected spike returns.* Journal of Applied Remote Sensing, 2010. **4**(1): p. 043549-043549-9.
158. Guan, Z., et al., *Insect monitoring with fluorescence lidar techniques: Field experiments.* Applied Optics, 2010. **49**(27): p. 5133-5142.

159. U. S. Navy Academy, *Naval Ordnance and Gunnery - Volume 2 - Fire Control*. 1955: U. S. Government Printing Office.
160. Darzynkiewicz, Z., M. Roederer, and H.J. Tanke, *Cytometry: new developments*. Methods in cell biology (Online): 75. 2004: Amsterdam ; Boston : Elsevier Academic Press, 2004.
161. Jericho, S.K., et al., *Submersible digital in-line holographic microscope.* Review of Scientific Instruments, 2006. **77**(4): p. 043706.
162. Scheimpflug, T., *Improved method and apparatus for the systematic alteration or distortion of plane pictures and images by means of lenses and mirrors for photography and for other purposes*, G. Patent, Editor. 1904.
163. Seeds, M.A. and D. Backman, *Stars and Galaxies*. 2015: Cengage Learning; 009 edition.
164. Brydegaard, M., *Towards Quantitative Optical Cross Sections in Entomological Laser Radar - Potential of Temporal and Spherical Parameterizations for Identifying Atmospheric Fauna.* PLoS ONE, 2015. **10**(8).
165. Brydegaard, M., et al., *Daily Evolution of the Insect Biomass Spectrum in an Agricultural Landscape Accessed with Lidar.* EPJ Web of Conferences, 2016. **119**: p. 22004.
166. Jr., W.H.O. and M.C. Kahn, *The Sounds of Disease-Carrying Mosquitoes.* The Journal of the Acoustical Society of America, 1949. **21**(3): p. 259-263.
167. Huang, H. and J. Pan, *Speech pitch determination based on Hilbert-Huang transform.* Signal Processing, 2006. **86**(4): p. 792-803.
168. Andersson, A., *Unbiasing entomological kHz Scheimpflug LIDAR data*, in *Department of Physics*. 2018, Lund University.
169. Villarreal, S.M., O. Winokur, and L. Harrington, *The Impact of Temperature and Body Size on Fundamental Flight Tone Variation in the Mosquito Vector Aedes aegypti (Diptera: Culicidae): Implications for Acoustic Lures.* Journal of Medical Entomology, 2017. **54**(5): p. 1116-1121.
170. Deakin, M.A.B., *Formulae for insect wingbeat frequency.* Journal of insect science (Online), 2010. **10**: p. 96-96.
171. Welch, P., *The use of fast Fourier transform for the estimation of power spectra: A method based on time averaging over short, modified periodograms.* IEEE Transactions on Audio and Electroacoustics, 1967. **15**(2): p. 70-73.
172. Beebe, K.R. and B.R. Kowalski, *An Introduction to Multivariate Calibration and Analysis.* Analytical Chemistry, 1987. **59**(17): p. 1007A-1017A.

173. Brydegaard, M., A. Runemark, and R. Bro, *Chemometric approach to chromatic spatial variance. Case study: patchiness of the Skyros wall lizard.* Journal of Chemometrics, 2012. **26**(6): p. 246-255.
174. Everitt, B.S., et al., *Cluster Analysis, 5th Edition*. 2011, Hoboken, NJ: Wiley.
175. Harrell, F.E., *Regression Modeling Strategies : With Applications to Linear Models, Logistic and Ordinal Regression, and Survival Analysis*. 2015, Cham, Switzerland: Springer.
176. Ballabio, D. and V. Consonni, *Classification tools in chemistry. Part 1: Linear models. PLS-DA.* Analytical methods, 2013. **5**: p. 3790-3798.
177. Warrant, E. and D.-E. Nilsson, *Invertebrate Vision*. 2006: Cambridge University Press; 1 edition.

Paper summaries and author contributions

Paper I:
First Polarimetric Investigation of Malaria Mosquitoes as Lidar Targets

S. Jansson, P. Atkinson, R. Ignell and M. Brydegaard
IEEE Journal of Selected Topics in Quantum Electronics **25**, 1-8 (2019).

In this paper, a laboratory measurement system was used to investigate the scattering properties of *Anopheles arabiensis* mosquitoes *ex-vivo*. The samples were investigated tomographically and goniometrically. The degree of linear polarization of mosquitoes was measured in forward- and backscatter mode, the aspect-dependent backscatter- and extinction OCS and the phase function of mosquitoes. It was determined that the degree of linear polarization of mosquito bodies is independent of the aspect angle, which corresponds to flight heading in lidar data. The 808 nm light that is commonly employed in entomological lidar is well suited for producing specular flashes of high magnitude in insect wings. It was also established that mosquitoes scatter predominantly in the forward direction. This work paves the way for flight heading models and is crucial for the interpretation of lidar field data, which may in turn have profound impact for vector control.

For this article I carried out the measurements, analysed the data, produced the figures and wrote most of the manuscript.

Paper II:
Multiband modulation spectroscopy for determination of sex and species of mosquitoes in flight

A. Gebru, **S. Jansson**, R. Ignell, C. Kirkeby, J. Prangsma and M.Brydegaard
Journal of Biophotonics **11**, e201800014 (2018).

For this paper, the scattering properties of males and females from four species of mosquitoes were investigated *in-vivo*. Free-flying mosquitoes were released into a

laser beam, and backscattered light was measured in two spectral- and two polarization bands. Apart from the polarization properties, this paper also shows that the spectral ratio between the NIR and the SWIR laser bands, which relates to the melanization of insects, are aspect-invariant. It is demonstrated that all investigated species and sexes of mosquitoes can be distinguished based on their spectral- and polarization properties in conjunction with dynamic properties such as the wing-beat frequency, including the closely related *Anopheles arabiensis* and *Anopheles coluzzii*. Additionally, it is shown that the optical cross sections of specular wing flashes enable the distinction of these two species of *Anopheles* mosquitoes, which is of particular interest for lidar applications since the magnitude of specular wing flashes does not decay with distance unlike other scattering parameters. Thereby, mosquito classification may be possible over very long distances.

For this article I aligned and calibrated the setup, carried out the measurements together with the first author, advised on the data analysis and contributed to the manuscript.

Paper III:
Correlation of mosquito wing-beat harmonics to aid in species classification and flight heading assessment

S. Jansson, A. Gebru, R. Ignell, J. Abbott and M. Brydegaard
Proceedings of SPIE **11075**, 110750Q (2019).

In this paper, the same dataset was used as in Paper II, and included an additional dataset of light scattered by fruit flies, *Drosophila melanogaster*. The details of the modulation spectra of all nine classes of insects were investigated. The correlation of the insect body signals and the modulation strengths of the lowest four harmonics were examined, and species specific patterns were observed. Wing-beat correlation is an important step towards devising a flight-heading model. A flight-heading model, in turn, may aid in the interpretation of field data, as the aspect-dependency of several classification parameters can be accounted for. Naïve Bayes classifiers were implemented with different sets of data, and it was demonstrated that all nine insect classes could be classified with high accuracy when data from both spectral- and both polarization bands were used. The classification accuracy was reduced significantly when only the co-polarized 808 nm band was used, corresponding to common entomological lidar conditions. When only the wing-beat frequency was used, the classification accuracy dropped even further, and many classes were confused for each other. This implies that multiple spectral- or polarization bands may be necessary for accurate mosquito classification in lidar

measurements, in conjunction with high sample rates to resolve mosquito wing beats.

For this article I aligned and calibrated the setup, carried out the measurements together with the second author, took part in conceiving the analysis method, analysed the data, produced the figures and wrote the manuscript.

Paper IV:
Can the narrow red bands of dragonflies be used to perceive wing interference patterns?

M. Brydegaard, **S. Jansson**, M. Schulz and A. Runemark
Ecology and Evolution **8**, 5369-5384 (2018).

In this paper we studied the optical properties of dragonflies (*Odonata*), and put them in relation to their visual bands. Dragonflies have the narrowest spectral bands reported in the animal kingdom, and we investigated what features these may be used to perceive. We present six lines of clues which indicate that the narrow red visual bands of dragonflies may enable them to perceive wing-interference patterns, and speculate on the ecological implications.

For this article I aligned and calibrated the setup used to retrieve modulation spectra in the laboratory, conducted the measurements on fruit flies, operated the lidar for the polarimetric field recordings of dragonflies in China and contributed to the manuscript.

Paper V:
Passive kHz lidar for the quantification of insect activity and dispersal

S. Jansson and M. Brydegaard
Animal Biotelemetry **6**, 6 (2018).

For the first time, we demonstrate passive ranging in the optical regime. A ranging equation was devised based on a raytracing simulation of a quadrant sensor's field of view. Field data from passive quadrant measurements was used to test the ranging equation, and the data matched the simulation well. The flight heading of insects was calculated and the flight speed was estimated, demonstrating that the method yields rich entomological information despite being inexpensive and simple in terms of instrumentation. The method has the potential to become a widespread tool for entomological monitoring. It can be implemented with active

illumination and may be scaled to fit the geometrical requirements of other applications.

For this article I carried out the simulations and developed the passive ranging method with the second author, analysed the data, produced the figures and wrote the manuscript. The work resulted in a patent where I am co-inventor.

Paper VI:
The Scheimpflug lidar method

M. Brydegaard, E. Malmqvist, **S. Jansson**, J. Larsson, S. Török and G. Zhao *Proceedings of SPIE* **10406**, 104060I (2017).

In this paper, the design parameters for Scheimpflug lidars are discussed and evaluated with raytracing. Different applications are briefly reviewed, and the performance of the method in each application is evaluated.

For this article I aided in the development of data processing algorithms of insect signals, set up and operated the lidar system during for field measurements resulting in figure 3 and 6, and contributed to the manuscript.

Paper VII:
Advances in entomological laser radar

M. Brydegaard and **S. Jansson**
The Journal of Engineering **2019**, 7542-7545 (2019).

This paper reviews some of the progress made in entomological lidar with regards to quantitative parameterization, target classification and laboratory reference measurements. An example of bee monitoring in relation to their hive is presented. For the first time, it is demonstrated that the wing beats of insects can be resolved by multiple shortwave infrared bands using time multiplexing. As demonstrated in Paper II-III, multiple spectral bands enable significantly improved prediction accuracy of classification models, which paves the way for species classification *in-situ*.

For this article I aided in the development of data processing methods, carried out the measurements resulting in figures 2-4, produced figure 3 and contributed to the manuscript.

Paper VIII:
Effective Parameterization of Laser Radar Observations of Atmospheric Fauna

E. Malmqvist, **S. Jansson**, S. Török and M. Brydegaard
IEEE Journal of Selected Topics in Quantum Electronics **22**, 1-8 (2016).

This paper details the first complete analysis process of entomological lidar data, by which insect observations are extracted from raw data and parameterized. It is shown how quantitative size estimates are obtained, and how the wing-beat frequencies of insects are determined. With the wing-beat frequency of insects known, the signal can be separated into the body- and wing- signal component. The strength and phase of the wing-beat frequency and higher harmonics is obtained through regression. By weighting the regressor with the signal envelope, the impact of the beam profile and insect transit time on the modulation spectrum, such as sidelobes, cancel out. Every step of the process is illustrated with lidar data from Brunslöv, Sweden, and most of the methodology is used to date.

For this article I aided in the development of the data processing, supplied feedback on the figures and contributed to the manuscript.

Paper IX:
Insect abundance over Chinese rice fields in relation to environmental parameters, studied with a polarization-sensitive CW near-IR lidar system

S. Zhu, E. Malmqvist, W. Li, **S. Jansson**, Y. Li, Z. Duan, K. Svanberg, H. Feng, Z. Song, G. Zhao, M. Brydegaard and S. Svanberg
Applied Physics B **123**, 211 (2017).

A novel polarimetric dual-band Scheimpflug lidar was used to study aerofauna over rice fields in Guangzhou, China. The insect activity was put into context relative to environmental parameters such as temperature and rain. Crepuscular activity peaks were observed each day. For the first time, insects could be distinguished from rain drops by their polarization properties. This enabled monitoring of insect activity during rainfall, and sharp activity peaks were observed at the onset of rain showers. These were interpreted as high-altitude migrants being washed down by the rain and forced to land.

For this article I aligned the system and carried out the measurements with the other authors, took part in discussions the on data analysis, produced figure 5 and contributed to the manuscript.

Paper X:
Risky bat bait – Insect swarm dynamics at a wind turbine observed with Scheimpflug lidar

S. Jansson, E. Malmqvist, M. Brydegaard, S. Åkesson and J. Rydell
In review

Each year, protected species of bats fly near wind farms to their demise as they are hit by the moving rotor blades. It is known that bats are attracted to wind farms during warm nights with low wind speed in August and September, but the reasons for their attraction is unknown. In this study an entomological lidar system was deployed next to a wind farm in southern Sweden to monitor the insect population vertically. Insect swarms were observed at the nacelle of the turbine most nights before sunset. On particularly warm nights, the swarming was prolonged until after sunset, overlapping with the activity hours of bats. On nights with particularly low wind speeds, swarms of larger insects were observed at the nacelle. Ultrasonic recordings indicate that bats are both feeding and courting at wind farms, and that both activities increase with higher insect counts. This implies that bats may be at wind farms to feed. Improved understanding of insect swarm dynamics at wind turbines may aid in reducing bat deaths in the future.

For this manuscript I aided in putting together the setup, planned and carried out the measurements with the second author, analysed the data, produced the figures and wrote the technical parts of the manuscript.

Paper XI:
The bat-bird-bug battle: daily flight activity of insects and their predators over a rice field revealed by high-resolution Scheimpflug Lidar

E. Malmqvist, **S. Jansson**, S. Zhu, W. Li, K. Svanberg, S. Svanberg, J. Rydell, Z. Song, J. Bood, M. Brydegaard and S. Åkesson
Royal Society Open Science **5**, 172303 (2018).

In this study a polarimetric Scheimpflug lidar system was used to the activity of birds, bats and insects, which has not been possible with any other method before. It is shown that the crepuscular activity peaks of insects were constrained into short time windows during which neither birds nor bats were present. The results indicate that flight behavior may be affected by predation risk.

For this article I carried out the measurements with the other authors, aided with the data analysis and contributed to the manuscript.

Paper XII:
Lidar reveals Activity Anomaly of Malaria Vectors during Pan-African Eclipse

M. Brydegaard, **S. Jansson**, E. Malmqvist, Y. Mlacha, A. Gebru, F. Okumu, G. Killeen and Carsten Kirkeby
In review

In this study we conducted entomological lidar measurements in a remote Tanzanian village during a solar eclipse. The modulation spectra of insects were investigated with hierarchical cluster analysis. Male and female mosquitoes were distinguished from other insects for the first time in entomological lidar field measurements. Further, the spatio-temporal activity patterns of malaria vectors were compared between regular days and the eclipse, during which an increased mosquito activity was observed. Thereby, the phototactic activity patterns were disentangled from the circadian mechanism of the mosquitoes. The results demonstrate that entomological lidar is a powerful tool with which an improved understanding of vector ecology may be gained.

For this manuscript I aided in the construction of the setup, planned the measurements with the first author and carried them out with all authors, developed algorithms for calibration and thresholding, analysed system stability and noise characteristics, supplied reference data on mosquitoes which aided the interpretation of field data and contributed to the manuscript.

Paper XIII:
Real-time dispersal of malaria vectors in rural Africa monitored with lidar

S. Jansson, E. Malmqvist, Y. Mlacha, R. Ignell, F. Okumu, G. Killeen, C. Kirkeby and M. Brydegaard
Submitted

In this study an entomological lidar system was deployed in the outskirts of Lupiro, a remote village in Tanzania. A 598 m transect 3-5 m above ground across an agricultural landscape was monitored for 3 full, consecutive days, observing 266330 insects flying through the laser beam. Male and female mosquitoes were distinguished from other insects using hierarchical cluster analysis, and the cluster interpretation was further validated with a separate frequency analysis method. Swarms of male mosquitoes were observed by the lidar consequently each night, at the same time and place. This has implications for vector control. Further, the

spatial distribution and dispersal of mosquitoes was found to differ significantly through the day, and a highly directed dispersal of female mosquitoes towards the village was observed each night.

For this manuscript I aided in the construction of the setup, planned the measurements with the last author and carried them out with all authors, developed thresholding methods, developed frequency analysis methods, analysed the data, produced the figures and wrote the manuscript.

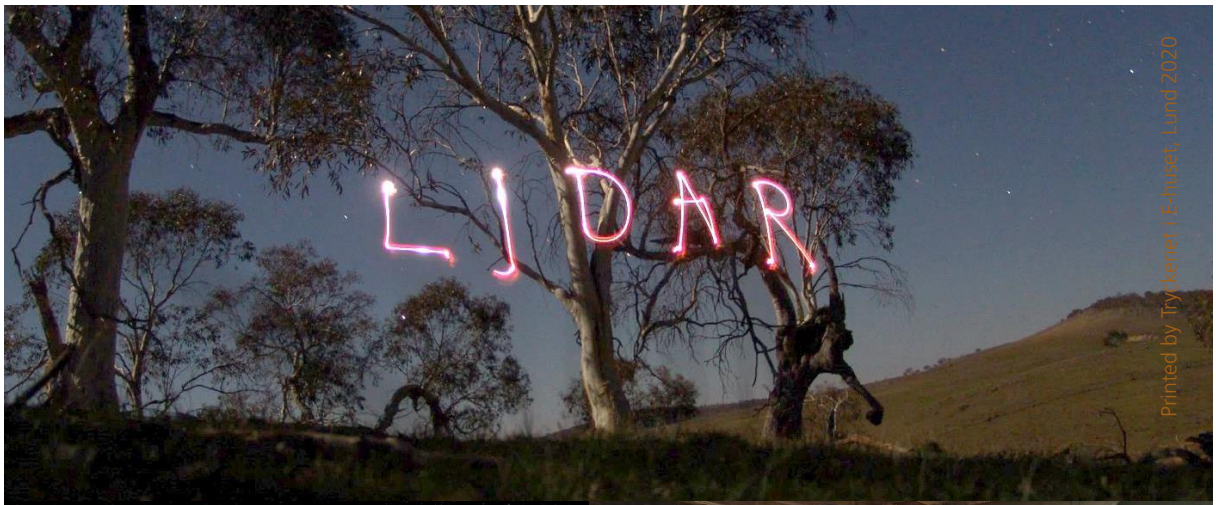

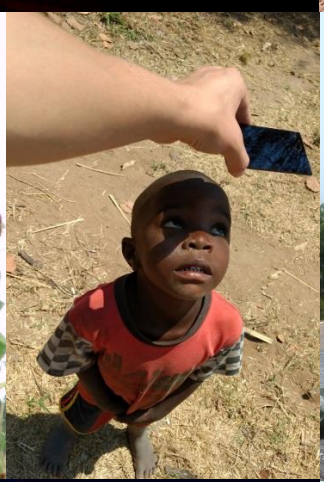

Printed by Tryckeriet i E-huset, Lund 2020

ISRN LUTFD2/TFCP-217-SE
ISSN 1102-8718

ISBN 978-91-7895-418-6 (PRINT)
ISBN 978-91-7895-419-3 (PDF)